


December 2017

## Synthesis and Electrochemical Characterization of PANI/Ni and PANI/Au/Ni Composites

Morgan Emily Pacini  
University of Nevada, Las Vegas, mejarvis4@gmail.com

Follow this and additional works at: <https://digitalscholarship.unlv.edu/thesesdissertations>

 Part of the [Inorganic Chemistry Commons](#), and the [Polymer Chemistry Commons](#)

---

### Repository Citation

Pacini, Morgan Emily, "Synthesis and Electrochemical Characterization of PANI/Ni and PANI/Au/Ni Composites" (2017). *UNLV Theses, Dissertations, Professional Papers, and Capstones*. 3158.  
<https://digitalscholarship.unlv.edu/thesesdissertations/3158>

This Thesis is protected by copyright and/or related rights. It has been brought to you by Digital Scholarship@UNLV with permission from the rights-holder(s). You are free to use this Thesis in any way that is permitted by the copyright and related rights legislation that applies to your use. For other uses you need to obtain permission from the rights-holder(s) directly, unless additional rights are indicated by a Creative Commons license in the record and/or on the work itself.

This Thesis has been accepted for inclusion in UNLV Theses, Dissertations, Professional Papers, and Capstones by an authorized administrator of Digital Scholarship@UNLV. For more information, please contact [digitalscholarship@unlv.edu](mailto:digitalscholarship@unlv.edu).

SYNTHESIS AND ELECTROCHEMICAL CHARACTERIZATION OF  
PANI/NI AND PANI/AU/NI COMPOSITES

By

Morgan Emily Pacini

Bachelor of Science – Biochemistry  
University of Nevada, Las Vegas  
2013

A thesis submitted in partial fulfillment  
of the requirements for the

Master of Science – Chemistry

Department of Chemistry and Biochemistry  
College of Sciences  
The Graduate College

University of Nevada, Las Vegas  
December 2017



## Thesis Approval

The Graduate College  
The University of Nevada, Las Vegas

November 7, 2017

This thesis prepared by

Synthesis and Electrochemical Characterization of PANI/Ni and PANI/Au/Ni  
Composites

entitled

Morgan Emily Pacini

is approved in partial fulfillment of the requirements for the degree of

Master of Science – Chemistry  
Department of Chemistry and Biochemistry

David Hatchett, Ph.D.  
*Examination Committee Chair*

Kathryn Hausbeck Korgan, Ph.D.  
*Graduate College Interim Dean*

Spencer Steinberg, Ph.D.  
*Examination Committee Member*

Bryan Spangelo, Ph.D.  
*Examination Committee Member*

Terry Spell, Ph.D.  
*Graduate College Faculty Representative*

## Abstract

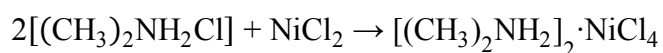
# Synthesis and Electrochemical Characterization of PANI/Ni and PANI/Au/Ni Composites

By

Morgan Emily Pacini

Dr. David W. Hatchett, Committee Chair  
Professor of Chemistry  
University of Nevada, Las Vegas

The purpose of this research is to show that the electrochemically controlled formation of monometallic and bimetallic catalysts in polyaniline (PANI) can directly influence the efficiency and reproducibility of the catalytic oxidation of methanol. PANI is a conductive polymer that provides a three-dimensional template for the metallic catalysts deposition at nitrogen sites. The controlled deposition of metallic species can be achieved using the normal oxidation/reduction cycles of PANI. The deposition of metallic species relies on anion precursors that are electrostatically bound by the polymer during the oxidation cycle. The precursor is reduced directly at the nitrogen sites in the polymer on the reverse cycle. While noble metal precursors such as  $\text{AuCl}_4^-$ ,  $\text{PdCl}_4^{2-}$  and  $\text{PtCl}_4^{2-}$  are available commercially, less expensive transition metal precursors were prepared in our lab. For example, the precursor  $\text{NiCl}_4^{2-}$  was prepared by reacting dimethylamine hydrochloride with  $\text{NiCl}_2$  in the presence of chloroform based on the following chemical reaction:



For proof of principal, solutions containing  $[(\text{CH}_3)_2\text{NH}_2]_2\cdot\text{NiCl}_4$  were utilized to achieve Ni deposits at graphitic electrodes prior to deposition in PANI. PANI/metallic catalysts containing single metal species including Au, Pd, and Pt are well known and have been the subject of many studies in our laboratory. However, it is clear from the previous results that significant poisoning of the catalyst occurs during the oxidation of methanol.<sup>1-6</sup> The byproducts of the oxidation reaction adsorb onto the metal surface poisoning or blocking further catalysis. However, PANI/bimetallic composite can be prepared providing better catalytic oxidation of alcohol with reduced poisoning of the metal catalyst surface. Bimetallic catalysts are achieved when nickel is electrochemically deposited onto gold in the polymer. The combination of two different metal species reduces the deposition of surface contaminants ensuring oxidation of methanol can occur at the catalyst surface. The bimetallic catalyst containing Ni rather than two noble metal species also reduces the cost associated with the oxidation of methanol. The controlled deposition of the bimetallic catalyst in PANI showed high reproducibility in solutions containing KOH and during methanol oxidation. The SEM/EDX analysis confirms the deposition of Au/Ni in PANI. Finally, PANI/Au/Ni composites show that surface poisoning is minimized in comparison to PANI/Au composites. However, PANI/Ni composites showed higher current density for methanol oxidation at Ni in comparison to PANI/Au/Ni composites.

## Acknowledgements

As my graduate journey comes to an end, I cannot begin to express how blessed I feel to have had the opportunity to learn from and work with incredible professors and peers. I would like to especially thank my advisor Dr. David Hatchett for giving me the opportunity to work in his research group as a Master's student and for believing in me and all that I could handle and accomplish. His guidance and support are truly appreciated.

I would also like to thank my committee members Dr. Spencer Steinberg, Dr. Bryan Spangelo, and Dr. Terry Spell, as well as Chemistry Department professors Dr. Vernon Hodge and Dr. Clemens Heske, who provided me with support and knowledge. I am truly thankful for having the opportunity to learn all that I could from all of them. My gratitude also goes out to Mark Miyamoto, Deborah Masters, Bianca Rideout, Mahin Behnia, and Carolyn Hatchett for all their guidance and assistance during my graduate research.

Prior to being accepted in the graduate program, I had the opportunity to work with amazing peers who helped guide me in the research lab. I would like to thank Bea Martinez, Janelle Droessler, and Nicole Goodwin for always supporting me and teaching me so much about all the instrumentation and techniques in the lab. I would also like to thank Nicole Millick, Kelly Zaugg, Jung Jae Koh, Katherine Thornock, and Cassara Higgins for all their support.

My gratitude further extends outside of UNLV to my family and friends. I would not have had the drive to finish or to accomplish all that I have without my biggest supporter, my incredible husband Mike Pacini. He has put up with so much including late nights of studying and writing, my complaints, and extremely stressful times where I did not know if I had the stamina to finish the Master's program. He was there throughout the process, by my side, always supporting me and encouraging me to persevere and to reach my goals. My parents,

grandparents, and my sister and brother-in-law also deserve a huge thank you for always believing in me and showing unconditional support. My mom and my sister have been great role models for me with all that they have accomplished, and without them, I would not have had the determination to pursue a Master's degree. In addition to my family, I would like to thank Rakesh Kothuru for his patience and support and all my friends for always having my back. Without having such amazing family members and friends, this journey would not have been possible.

## Table of Contents

Abstract .....	iii
Acknowledgements .....	v
List of Tables .....	ix
List of Figures .....	x
Chapter 1: Introduction .....	1
1.1 Motivation .....	1
1.2 Background, Synthesis, and Applications for PANI .....	2
1.3 PANI and the Incorporation of Secondary Components .....	4
1.3.1 PANI/Noble Metal Composites vs PANI/Transition Metal Composites .....	7
1.4 PANI/Bimetallic Composites.....	8
1.5 Organization of Thesis .....	9
Chapter 2. Experimental Methods .....	11
2.1 Synthesis of Metal Precursors.....	11
2.1.1 Chemicals and Solutions.....	11
2.1.2 Bis(dimethylammonium) Hexachlorotitanate, $[(\text{CH}_3)_2\text{NH}_2]_2 \cdot \text{TiCl}_6$ .....	12
2.1.3 Bis(dimethylammonium) Tetrachloronickelate, $[(\text{CH}_3)_2\text{NH}_2]_2 \cdot \text{NiCl}_4$ .....	13
2.1.4 Bis(dimethylammonium) Tetrachlorogallinate, $[(\text{CH}_3)_2\text{NH}_2] \cdot \text{GaCl}_4$ .....	15
2.2 Instrumental Analysis .....	16
2.2.1 Fourier-Transform Infrared Spectroscopy (FT-IR) .....	16
2.2.2 UV/Vis Spectroscopy Analysis.....	17
2.2.3 Powder X-Ray Diffraction (XRD) Analyses .....	18
2.2.4. Electrochemical Apparatus and Conditions.....	20
2.2.5 Scanning Electron Microscopy (SEM)/Energy Dispersive Spectroscopy (EDS)...	20
Chapter 3. Characterization and Electrochemical Analysis of PANI/Ni Composites .....	22
3.1 Introduction.....	22
3.2 Characterization of Ni Precursors .....	22
3.2.1 FTIR Spectroscopy of Ni Precursors .....	22
3.2.2 UV/Vis Spectroscopy of Ni Precursors .....	25
3.2.3 Powder X-Ray Diffraction of Ni Precursors.....	27



3.3 Electrochemical Synthesis of Ni Composites .....	28
3.3.1 Ni Electrochemistry on Grafoil.....	28
3.3.2 SEM/EDX Ni on Grafoil .....	29
3.3.3 Grafoil/Ni Electrochemistry in KOH.....	31
3.3.4 Grafoil/Ni Electrochemistry in CH <sub>3</sub> OH/KOH.....	33
3.4 Electrochemical Analysis of PANI/Ni Composites .....	35
3.4.1 Electrochemical Synthesis of PANI.....	35
3.4.2 Ni Deposition in PANI.....	36
3.4.3 Proton Dope Analysis of PANI/Ni Composite .....	37
3.4.4 Scanning Electron Microscopy (SEM/EDX) of PANI/Ni Composites .....	39
3.4.5 PANI/Ni Electrochemistry in KOH.....	41
3.4.6 PANI/Ni Electrochemistry in CH <sub>3</sub> OH/KOH .....	42
3.4.7 PANI/NiCl <sub>2</sub> Electrochemistry in KOH versus PANI/Ni Precursor.....	46
3.4.8 PANI/NiCl <sub>2</sub> Electrochemistry versus PANI/NiCl <sub>4</sub> in 1 M CH <sub>3</sub> OH/KOH.....	48
3.5 Conclusions.....	49
Chapter 4. Electrochemical Formation and Analysis of PANI/Au/Ni Composites .....	52
4.1 Introduction.....	52
4.2 Electrochemical Formation of PANI/Au/Ni Composites .....	52
4.2.1 Sequential Deposition of Gold and Nickel in PANI.....	52
4.2.2 Proton Dope Analysis of PANI/Au/Ni Composite .....	54
4.3 Scanning Electron Microscopy (SEM/EDX) of PANI/Au/Ni Composites .....	56
4.4 Electrochemical Analysis of PANI/Au/Ni Composites .....	59
4.4.1 PANI/Au/Ni Electrochemical Analysis in KOH .....	59
4.4.2 PANI/Au/Ni Electrochemical Analysis in 1 M CH <sub>3</sub> OH/KOH .....	61
4.5 Comparison of Catalytic Activity of PANI/Metallic Composites .....	63
4.5.1 Stability of Bimetallic Catalysts .....	63
4.5.2 Comparison of Methanol Oxidation for All Composites.....	65
4.6 Conclusions.....	67
Chapter 5. Summary and Conclusions.....	69
References.....	72
Curriculum Vitae .....	77

## List of Tables

<b>Table 1.</b> Far-Infrared Absorption Frequencies ( $\text{cm}^{-1}$ ) obtained for the starting compounds and for the Ni precursor .....	23
---	----

## List of Figures

<b>Figure 1.</b> The electrochemical oxidation of aniline <sup>14</sup> .....	3
<b>Figure 2.</b> Acid doping of PANI <sup>18</sup> .....	4
<b>Figure 3.</b> AuCl <sub>4</sub> <sup>-</sup> anion uptake and reduction in PANI <sup>1, 18</sup> .....	6
<b>Figure 4.</b> Titanium precursor, [(CH <sub>3</sub> ) <sub>2</sub> NH <sub>2</sub> ] <sub>2</sub> ·TiCl <sub>6</sub> , after being dried in a desiccator. ....	13
<b>Figure 5.</b> The starting NiCl <sub>2</sub> material (left) versus the synthesized Ni precursor (right).....	14
<b>Figure 6.</b> The synthesized gallium precursor, [(CH <sub>3</sub> ) <sub>2</sub> NH <sub>2</sub> ] <sub>2</sub> ·GaCl <sub>4</sub> . ....	16
<b>Figure 7.</b> FTIR photoacoustic response of the starting components (a) NiCl <sub>2</sub> and (b) (CH <sub>3</sub> ) <sub>2</sub> NH <sub>2</sub> Cl, and of the synthesized (c) Ni Precursor, [(CH <sub>3</sub> ) <sub>2</sub> NH <sub>2</sub> ] <sub>2</sub> ·NiCl <sub>4</sub> . ....	23
<b>Figure 8.</b> UV/Vis absorbance spectrum for 50 mM NiCl <sub>4</sub> <sup>2-</sup> (solid line) and 50 mM NiCl <sub>2</sub> (dashed line) in H <sub>2</sub> O. ....	25
<b>Figure 9.</b> UV/Vis absorbance spectra for 50 mM NiCl <sub>4</sub> <sup>2-</sup> (solid line) and 50mM NiCl <sub>2</sub> (dashed line) in ionic liquid.....	26
<b>Figure 10.</b> Powder XRD of Ni Precursor, [(CH <sub>3</sub> ) <sub>2</sub> NH] <sub>2</sub> ·NiCl <sub>4</sub> , in comparison to powder XRD of the starting Ni component, NiCl <sub>2</sub> .....	27
<b>Figure 11.</b> Sweep-step function voltammetric response of (a) first step scan of 50 mM NiCl <sub>4</sub> <sup>2-</sup> deposited on grafoil, (b) second step scan of 50 mM NiCl <sub>4</sub> <sup>2-</sup> deposited on grafoil (c) third step scan of 50 mM NiCl <sub>4</sub> <sup>2-</sup> deposited on grafoil, (d) fourth step scan of 50 mM NiCl <sub>4</sub> <sup>2-</sup> deposited on grafoil, (e) fifth step scan of 50 mM NiCl <sub>4</sub> <sup>2-</sup> deposited on grafoil.....	29
<b>Figure 12.</b> SEM image and EDX data of (a) grafoil (x600, 20kV) and (b) 5 sweep step depositions of 50 mM NiCl <sub>4</sub> <sup>2-</sup> on grafoil (x450, 20kV).....	30

**Figure 13.** Steady-state cyclic voltammetric response of (a) Ni disc electrode (3mm), (b) response of Grafoil electrode (c) response of Grafoil/1 Ni and Grafoil/5 Ni after the 10<sup>th</sup> voltammetric scan in solution containing 1 M KOH. .... 32

**Figure 14.** Steady-state cyclic voltammetric response of (a) Ni disc electrode (3mm), (b) Grafoil electrode (c) Grafoil/1 Ni (d) Grafoil/3 Ni, and (e) Grafoil/5 Ni after the sixteenth voltammetric scan in solutions containing 1 M KOH and 1 M CH<sub>3</sub>OH. .... 35

**Figure 15.** Steady-state cyclic voltammetric response of PANI growth on grafoil (working area=1.2 cm<sup>2</sup>) after the first (dotted line) and twentieth (solid line) scan; scan rate is 10 mV/s. . 36

**Figure 16.** Sweep-step function voltammetric response of (a) first step scan of 50 mM NiCl<sub>4</sub><sup>2-</sup> deposited on PANI, (b) third step scan of 50 mM NiCl<sub>4</sub><sup>2-</sup> deposited on PANI, and (c) fifth step scan of 50 mM NiCl<sub>4</sub><sup>2-</sup> deposited on PANI. .... 37

**Figure 17.** Comparison of proton dopes of (a) PANI growth, and (b) PANI/Ni after the tenth voltammetric scan in 1 M HClO<sub>4</sub>. .... 39

**Figure 18.** SEM image and EDX data of (a) PANI (x20,000, 8.0kV) and (b) 5 sweep step depositions of 50 mM NiCl<sub>4</sub><sup>2-</sup> on PANI on grafoil (x20,000, 8.0kV). .... 41

**Figure 19.** Steady-state cyclic voltammetric response of (a) Ni disc electrode (3mm), (b) response of PANI on grafoil (c) response of PANI/1 Ni, (d) response of PANI/3 Ni, and (e) response of PANI/5 Ni after the tenth voltammetric scan in solutions containing 1 M KOH; scan rate is 10mV/s. .... 42

**Figure 20.** Steady-state cyclic voltammetric response of (a) response of Ni disc electrode (3mm), (b) PANI on grafoil electrode, (c) response of PANI/1 Ni, (d) response of PANI/3 Ni, and (e) response of PANI/5 Ni after the sixteen voltammetric scan in solutions containing 1 M KOH and 1 M CH<sub>3</sub>OH; scan rate is 10mV/s. .... 44

**Figure 21.** Steady-state cyclic voltammetric response of PANI/5 Ni after the sixteenth (solid line) and one-hundredth (dashed line) voltammetric scan in solutions containing 1 M KOH and 1 M CH<sub>3</sub>OH. .... 45

**Figure 22.** Steady-state, cyclic voltammetric response of (a) PANI/5 steps of 50 mM NiCl<sub>2</sub> and (b) response of PANI/5 steps of 50 mM NiCl<sub>4</sub><sup>2-</sup> after the tenth voltammetric scan in solutions containing 1 M KOH. .... 47

**Figure 23.** Steady-state cyclic voltammetric response of (a) PANI/5 steps of 50 mM NiCl<sub>2</sub> and (b) response of PANI/5 steps of 50 mM NiCl<sub>4</sub><sup>2-</sup> after the sixteenth voltammetric scan in solutions containing 1 M CH<sub>3</sub>OH/KOH..... 49

**Figure 24.** LSV voltammetric response of the 1<sup>st</sup> and only step scan of 5 mM AuCl<sub>4</sub> deposited on PANI on Grafoil (dotted line) and of the 1<sup>st</sup> of five step scans of 50 mM NiCl<sub>4</sub> deposited on PANI/Au (solid line)..... 54

**Figure 25.** Comparison of proton dopes of (a) PANI growth, (b) PANI/1 Au, and (c) PANI/1Au/5Ni after the tenth voltammetric scan in 1 M HClO<sub>4</sub>..... 55

**Figure 26.** SEM image and EDX analyses of (a) pristine PANI (×6000), (b) PANI/1 Au composite (x6000), and (c) PANI/1Au/5 Ni composite (x6000)..... 57

**Figure 27.** SEM image of PANI/Au/Ni composites at a magnification of x35,000. .... 58

**Figure 28.** Steady-state cyclic voltammetric response of (a) a planar Au disc electrode (d=3mm), (b) PANI on grafoil, (c) PANI/1Au composite, (d) PANI/1Au/1Ni composite, (e) PANI/1Au/3Ni composite, (f) PANI/1Au/5Ni composite, (g) a planar Ni disc electrode (d=3mm) after the tenth voltammetric scan in solution containing 1 M KOH. .... 60

**Figure 29.** Steady-state cyclic voltammetric response of (a) a planar Au disc electrode, (b) PANI on grafoil, (c) PANI/1Au composite, (d) a planar Ni disc electrode, (e) PANI/1Au/1Ni

composite, (f) PANI/1Au/3Ni composite, (g) PANI/1Au/5Ni composite after the sixteenth voltammetric scan in solution containing 1 M CH<sub>3</sub>OH/KOH. .... 63

**Figure 30.** Steady-state cyclic voltammetric response of (a) Ni disc electrode (d=3mm) and (b) response of PANI/1 Au/5 Ni after the sixteenth (solid line) and one-hundredth (dashed line) voltammetric scan in solutions containing 1 M KOH and 1 M CH<sub>3</sub>OH ..... 65

**Figure 31.** Steady-state cyclic voltammetric response of (a) a planar Ni disc electrode (b) Grafoil/5Ni electrode (c) Grafoil/PANI/1Au/5Ni composite, and (d) Grafoil/PANI/5Ni composite after the sixteenth voltammetric scan in solution containing 1 M CH<sub>3</sub>OH/KOH.. ..... 66

## Chapter 1: Introduction

### 1.1 Motivation

Electrochemical methods are utilized to produce Polyaniline (PANI)/metallic composites with unique or novel properties relative to the individual components. The preparation methods can dramatically influence their chemical and physical properties of the PANI/metallic composites. The research in this thesis focused to explore different metal species that can be exploited for the electrochemical preparation of PANI/metallic composites with enhanced catalytic properties. The goal is to replace more expensive metal catalysts including Au, Pd, and Pt with transition metals including Ni and Ga. The first part of this thesis will focus on the chemical synthesis of three different transition metal precursors containing a dimethylammonium cation and a metal chloride anion. The three metal chloride anions included tetrachloronickelate ( $\text{NiCl}_4^{2-}$ ), hexachlorotitanate ( $\text{TiCl}_6^{2-}$ ), and tetrachlorogallate ( $\text{GaCl}_4^-$ ). Although multiple metal precursors are produced, the second portion of the thesis is focused on the characterization of the Ni precursor and the electrochemically controlled uptake and reduction of  $\text{NiCl}_4^{2-}$  in PANI to form PANI/Ni composites. Finally, the last portion of the thesis is focused on the formation of PANI/Au/Ni composites. Following the formation PANI/Ni and PANI/Au/Ni composites the catalytic oxidation of methanol was utilized to probe metal specific chemical interactions and reactions. The hypothesis that will be explored is focused on determining if the oxidation of PANI can be utilized to control anion uptake and reduction of metallic precursors to achieve highly dispersed, high surface area, single metallic (Ni) and bimetallic (Au/Ni) composites with well-defined catalytic properties.

## 1.2 Background, Synthesis, and Applications for PANI

Polyaniline (PANI) is a well-studied conductive polymer that is formed using either chemical or electrochemical methods to oxidize aniline.<sup>2, 7</sup> Polymerization is initiated through the oxidation of the aniline monomer and formation of the aniline radical. There are obvious advantages and disadvantages of preparing PANI using either chemical or electrochemical synthesis methods.<sup>2, 7-12</sup> Bulk synthesis of PANI is achieved chemically by combining the aniline monomer with oxidant ammonium peroxydisulfate in an acidic solution.<sup>8</sup> Bulk chemical synthesis produces PANI with variable molecular weight and trapped oligomeric materials. In addition, the polymer composition can be variable because the chain length and oxidation state of the material is not easily controlled during chemical synthesis. In contrast, the electrochemical synthesis of PANI can be initiated through the potential dependent oxidation of the aniline monomer. Electrochemical methods allow the rate of reaction and oxidation potential to be precisely controlled, which influences the overall homogeneity while simultaneously minimizing incorporation of low molecular weight oligomers (**Figure 1**).<sup>8-9, 13-14</sup>



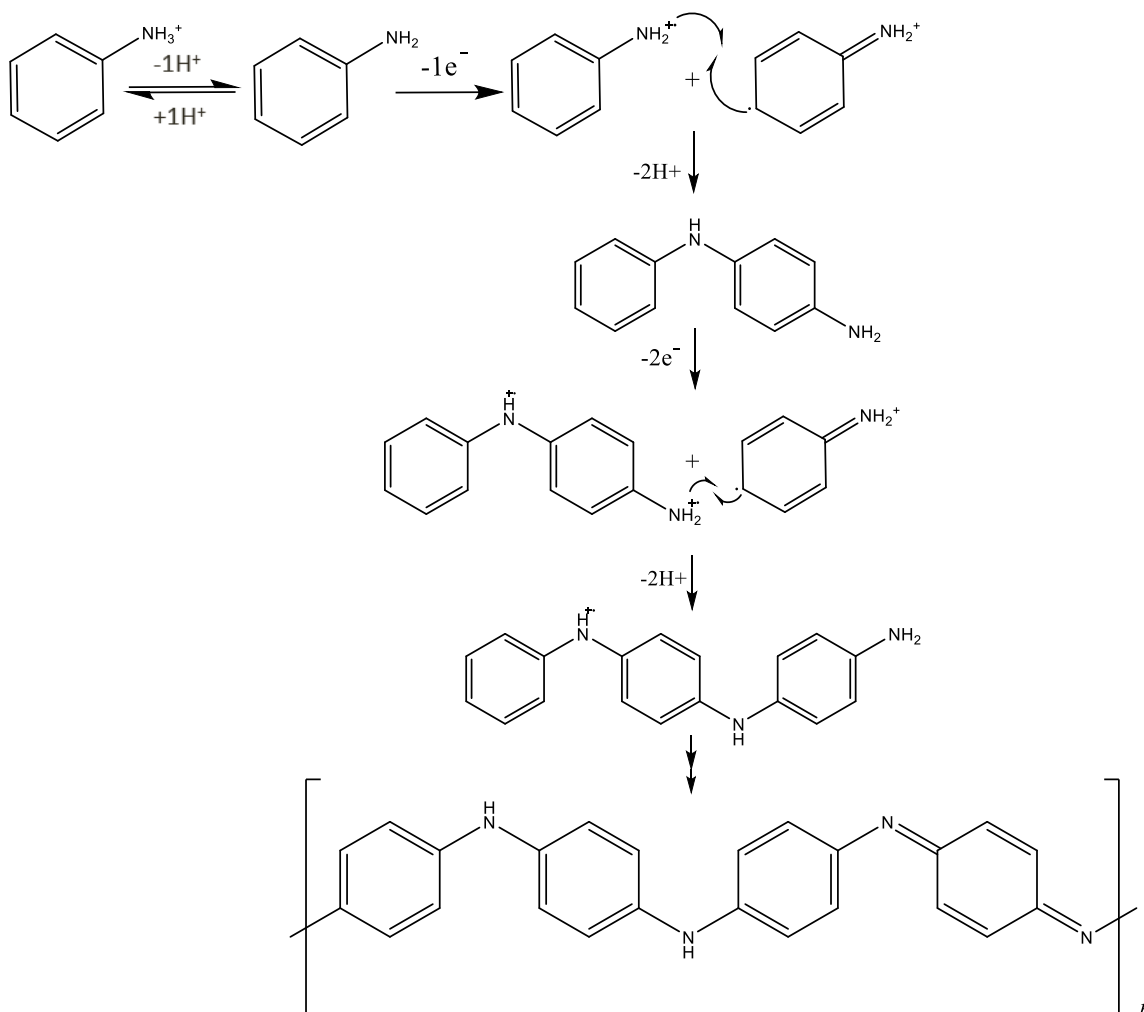


**Figure 1.** The electrochemical oxidation of aniline<sup>14</sup>

The basic structure of PANI contains repeated units of benzenoid (reduced) and the quinoid (oxidized) groups, which can be varied in the presence of an applied potential or chemical oxidant/reductant.<sup>7</sup> The emeraldine base form of PANI is made up of equal amounts of oxidized and reduced groups with the conductivity influenced by both the oxidation state of the polymer and proton doping of the nitrogen groups. The oxidation/reduction of PANI influences the nitrogen groups in the polymer through the conversion of imine and amine functionalities. In addition, the uptake and expulsion of protons and anions occur as the polymer is reduced and oxidized to maintain charge neutrality.<sup>10, 12-13, 15</sup> Proton uptake at the imine sites in the partially

oxidized polymer produces the emeraldine salt, which is the most conductive form of the polymer.<sup>7, 16</sup> Proton uptake at neutral imine groups at low pH can also occur producing positive charge within PANI, which is offset by the uptake of anion species from the solution (**Figure 2**).<sup>2, 10, 12, 17</sup> Finally, the electronic properties of the polymer can be further influenced by secondary doping of additional chemical species.<sup>18</sup> The incorporation of secondary species can be achieved using methods that are both independent and coupled to the oxidation/reduction of the polymer and proton/anion uptake.

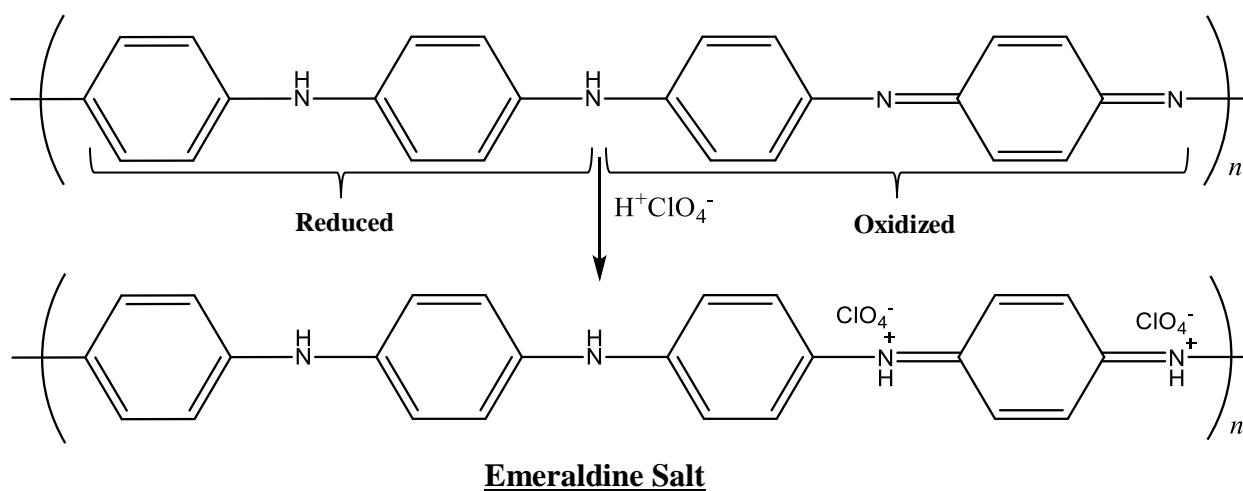


**Figure 2.** Acid doping of PANI<sup>18</sup>

### 1.3 PANI and the Incorporation of Secondary Components

The incorporation of secondary components into PANI can be achieved through two distinct pathways, which can be divided into spontaneous or controlled chemical reactions. Both methods have been used to produce PANI composites containing metal, metal oxide, and carbon materials. The variable electronic and chemical properties produced from different composite compositions can be exploited in a wide variety of chemical sensing and catalytic applications.<sup>19</sup>

The different synthetic approaches share the common goal of producing composites with uniformly dispersed secondary species with high surface area and reactivity in PANI. For example, the spontaneous reaction of secondary metallic species in PANI can be achieved by immersing PANI in either cation or anion solutions.<sup>7</sup> The process does not allow dispersion within the polymer because diffusion is minimized in spontaneous processes. In addition, spontaneous reduction of metal species occurs at the outermost surface, which produces PANI/metal composites with high metal aggregation. The process reduces the overall metal surface area of the secondary species.<sup>20</sup> In addition, the spontaneous reduction of metal ceases as the polymer becomes more oxidized. Inclusion of metal capping agents such as polyvinylpyrrolidone (PVP) or citrate can reduce aggregation within the polymer. However, adsorption of the capping agents onto the metal also blocks the metal surface, which reduces reactions at the surface. Therefore, they must be removed from the metal surface to achieve the highest chemical reactivity or efficiency as a catalyst.<sup>20-21</sup>

A synthetic pathway that allows the chemical reactivity of the polymer and secondary species to be precisely controlled is preferable in comparison to spontaneous chemical reactions. Electrochemical methods can be used to change the oxidation/reduction of PANI influencing both the uptake and dispersion of secondary species in the polymer. In addition, the controlled electrochemical reduction of secondary species after uptake and dispersion allows the composition of the PANI/metal composites to be precisely controlled and varied.<sup>2, 11-12</sup> The electrochemical method utilizes electrochemically formed PANI membranes as a substrate for anion precursor uptake and reduction through the normal oxidation and reduction of the polymer.<sup>2, 18, 22-23</sup> The uptake and dispersion of secondary species is achieved as the polymer is oxidized and electrostatic interactions between the oxidized polymer and anion are formed. The

anion precursor is subsequently reduced as the polymer is cycled to more negative potentials to produce the composite.<sup>2, 24</sup> The reduction process can produce metal or metal oxide deposits depending on the species. Noble metal precursors containing Au, Pt, and Pd produce metallic deposits.<sup>1-2, 18, 22-23</sup> In contrast, Ni and Ti transition metal precursors produce metal oxide deposits. The oxidative dissolution of the metals in PANI is minimized on subsequent oxidative cycles for both metal and metal oxide deposits. For example, **Figure 3** goes through the processes for the uptake and reduction of  $\text{AuCl}_4^-$  in PANI.<sup>1</sup> The processes can be repeated where additional electrochemical cycles increase the overall metal content in the polymer. Composites formed using electrochemical methods have unique physical properties relative to pristine PANI. For example, previous studies have shown that uptake of ~20% by weight metal (Au, Pd, Pt) allow the PANI/metal composite materials to be utilized in highly alkaline solutions that preclude proton doping.<sup>1-2, 10, 12, 18</sup>

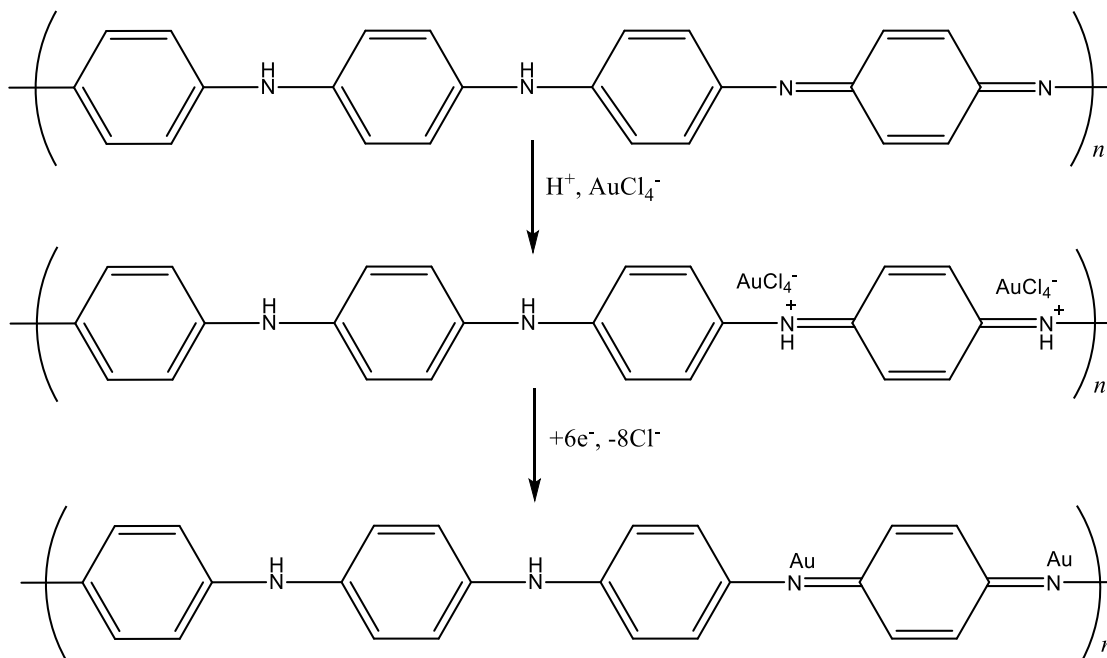


**Figure 3.**  $\text{AuCl}_4^-$  anion uptake and reduction in PANI<sup>1, 18</sup>

### 1.3.1 PANI/Noble Metal Composites vs PANI/Transition Metal Composites

The electrochemical uptake and reduction of noble metal precursors in PANI has included species such as  $\text{PtCl}_4^{2-}$ ,  $\text{PtCl}_6^{2-}$ ,  $\text{PdCl}_4^{2-}$ ,  $\text{PdCl}_6^{2-}$  and  $\text{AuCl}_4^-$ .<sup>1-2, 19</sup> Previous studies of PANI/metal composites such as PANI/Au, PANI/Pd, and PANI/Pt have focused on catalytic alcohol oxidation.<sup>1-2, 10, 12, 16, 19</sup> However, the noble metal precursors are susceptible to surface poisoning which reduces the overall catalytic efficiency.<sup>1-2, 19, 25</sup> In addition, the costs associated with noble metal precursors is high. Therefore, many studies have examined lower cost transition metal species for catalysis such as zinc, manganese, iron, cobalt, nickel, and copper to improve oxygen reduction reaction (ORR) activity for proton exchange membrane fuel cells (PEMFCs) as well as to improve methanol oxidation for direct methanol fuel cells (DMFCs).<sup>26-31</sup> Generally, the composites are produced utilizing cation species dissolved in acidic solution.<sup>24, 26, 28-29, 32-33</sup> For example, PANI/Ni and PANI/Cu composites have been formed in boric acid solutions containing  $\text{NiSO}_4$  and  $\text{CuSO}_4$ .<sup>24, 33</sup> The PANI/Cu composites that were formed using acidic solutions containing the metal cation precursor did not result in appreciable methanol oxidation. The addition of more noble metals to the PANI/Cu composites resulted in measurable methanol oxidation. In contrast, PANI/Ni composites achieved methanol oxidation without the addition of additional metal species. Although the formation of PANI/Ni and Cu composites was demonstrated, the reduction of the metal cation required significant reduction potentials in acidic environments to be achieved (Ni ~ -1.2 V vs. SCE and Cu ~ -0.2 V vs. SCE). The reduction potentials utilized in these studies are problematic because hydrogen evolution decreases the efficiency of deposition. Additional studies have examined PANI/metal composite formation using various transition metal chlorides such as  $\text{NiCl}_2$ ,  $\text{CdCl}_2$ , and  $\text{ZnCl}_2$ .<sup>32</sup> These studies did not result in the formation of PANI/metal composites. Rather, a bridge complex was formed between

the metal species and PANI. The results suggest that metal cation species cannot be spontaneously reduced by PANI to form a metal composite. Electrochemical methods were not utilized in these studies to reduce the metal cation further to form PANI/metallic composites. The controlled electrochemical reduction of anion precursors to produce highly dispersed and reactive transition metal species in PANI are favored over more traditional cation reduction pathways.

#### 1.4 PANI/Bimetallic Composites

The inclusion of bimetallic species in PANI for the improvement of methanol oxidation has also been explored using various PANI/bimetallic species such as PANI/PtPd, PANI/AgPt, PANI/LaCd, PANI/CoCu, PANI/PdNi.<sup>5-6, 34-36</sup> Bimetallic species in PANI can help to reduce surface poisoning that can occur during the oxidation of alcohols and they are known to have enhanced properties.<sup>5-6, 34-37</sup> Previous studies of Pd/Ni bimetallic composites showed increased catalytic activity towards alcohol oxidation with reduced surface poisoning.<sup>36</sup> However, oxidation of methanol at Pd was higher when compared to Pd/Ni composites. In these studies, Ni formed a small shell around the Pd, which reduced competing processes such as oxygen evolution reaction (OER) and the formation of CO adsorbed by methanol oxidation.<sup>36</sup> In addition, PANI/Pd/Ni composites showed increased methanol oxidation when compared to Pd/Ni bimetallic composites deposited on a two dimensional surface. The three dimensional structure of the polymer increases surface area and active sites while also reducing poisoning of the metal surface to allow more effective methanol oxidation.<sup>38</sup> The data suggests that formation of bimetallic catalysts in PANI can be used to optimize methanol oxidation and increase catalytic efficiency.

The efficiency of bimetallic catalysts has been explored to increase the efficiency of alcohol oxidation. In particular, AuNi bimetallic catalysts have shown increased methanol oxidation versus gold alone.<sup>39</sup> As a single metal, research on gold has shown that a small amount of methanol oxidation occurs through adsorbed –OH on the surface of the gold.<sup>4</sup> To enhance the catalytic oxidation of methanol, Ni has been incorporated due to its ability to form NiOOH during methanol oxidation which facilitates to oxidize adsorbed CO to yield CO<sub>2</sub>. CO is the cause of Au surface poisoning during the electrooxidation of methanol which severely limits the process. Therefore, AuNi species can have improved catalytic efficiency based on a bifunctional mechanism.<sup>39</sup> The mechanism suggests that the inclusion of Ni and Au will reduce surface poisoning while providing higher surface areas using the three-dimensional surface of the polymer to improve methanol oxidation.

### 1.5 Organization of Thesis

The current research utilized electrochemical methods to control the uptake, dispersion, and reduction of the NiCl<sub>4</sub><sup>2-</sup> to form PANI/Ni composites. The deposition of NiCl<sub>4</sub><sup>2-</sup> is demonstrated and the PANI/Ni composites are evaluated using Scanning Electron Microscopy (SEM) and Energy Dispersive X-ray Spectroscopy (EDS). Furthermore, the electrochemical properties of Ni in the polymer are examined using specific electrochemical reactions. The oxidation/reduction of Ni oxide and methanol oxidation in alkaline solutions are utilized to probe the metallic species in the PANI/Ni composites. Furthermore, all electrochemical experiments are conducted in alkaline solutions to ensure that the conductivity of the PANI/Ni composite is not reliant on acid doping of the polymer.

The electrochemical sequential deposition of AuCl<sub>4</sub><sup>-</sup> and NiCl<sub>4</sub><sup>2-</sup> is utilized for the formation of PANI/Au/Ni composites. The PANI/Au/Ni composites are also evaluated using

Scanning Electron Microscopy (SEM) and Energy Dispersive X-ray Spectroscopy (EDS). Furthermore, methanol oxidation in alkaline solutions is demonstrated.

Chapter 2 will consist of a summary of chemicals and solutions utilized to complete this research. A summary of the synthesis of each of the transition metal precursors will also be provided in Chapter 2 along with the explanation of each of the instruments utilized to analyze the Ni precursor, specifically. The electrochemical methods and parameters for the growth of PANI, deposition of Ni in PANI, formation of PANI/Au/Ni composites, and the electrochemical analytic oxidation of methanol using the PANI composites will be discussed as well in this chapter. Chapter 3 and Chapter 4 will provide an overview for the results and discussions relative to PANI/Ni and PANI/Au/Ni composites. Finally, Chapter 5 will provide an overall summary of the research in this thesis and possible future research.



## Chapter 2. Experimental Methods

This chapter provides a summary of the synthesis of three transition metal precursors,  $[(\text{CH}_3)_2\text{NH}_2]_2 \cdot \text{TiCl}_6$ ,  $[(\text{CH}_3)_2\text{NH}_2]_2 \cdot \text{GaCl}_4$ , and  $[(\text{CH}_3)_2\text{NH}_2]_2 \cdot \text{NiCl}_4$ , and it includes chemicals and solutions utilized for these stoichiometric reactions. In addition, an overview is provided for each instrument utilized for the characterization of these metal precursors as well as those used for the formation and characterization of the PANI/metallic composites. More detailed information and parameters will be given in the following chapters where they are applicable.

### 2.1 Synthesis of Metal Precursors

#### 2.1.1 Chemicals and Solutions

All solvents and compounds were purchased from VWR International and utilized without further purification for the synthesis of the metal precursors. Dimethylamine hydrochloride,  $(\text{CH}_3)_2\text{NH} \cdot \text{HCl}$ , was obtained from Acros Organics (99%). This was the cation utilized for the synthesis of the metal precursors. The titanium precursor was synthesized using titanium (IV) chloride,  $\text{TiCl}_4$ , supplied by Strem Chemicals Inc. (99.8%). Nickel (II) chloride anhydrous,  $\text{NiCl}_2$ , was supplied by Alfa Aesar (99%) and was utilized for the synthesis of the nickel precursor. The gallium precursor was made using gallium (III) chloride, anhydrous,  $\text{GaCl}_3$ , which was provided by Strem Chemicals Inc. (99.999%-Ga). Chloroform,  $\text{CHCl}_3$ , supplied by VWR (99.8%) was the solvent exploited during the synthesis of the three metal precursors. All synthesis reactions were conducted in a polyethylene glove bag purchased through VWR. The bag was subjected to a positive pressure of ultra-high purity dried nitrogen supplied by Air Gas (99.9999%).

### 2.1.2 Bis(dimethylammonium) Hexachlorotitanate, $[(\text{CH}_3)_2\text{NH}_2]_2 \cdot \text{TiCl}_6$

The synthesis of bis(dimethylammonium) hexachlorotitanate was carried out using the following reaction:



The procedure for the synthesis of the Ti precursor was taken from previously published research in 2002 by Rannabauer et al.<sup>40</sup> Originally,  $(\text{CH}_3\text{SiNH})_2\text{SiClINCH}_2$  was reacted with  $\text{TiCl}_4$  to form the by-product  $[(\text{CH}_3)_2\text{NH}_2]_2 \cdot \text{TiCl}_6$ . However, it was concluded that reacting dimethylamine hydrochloride with  $\text{TiCl}_4$  at room temperature in  $\text{CHCl}_3$  produced a higher yield of the required product.<sup>40</sup> Therefore, the synthesis was carried out using the following method. 1 gram of  $[(\text{CH}_3)_2\text{NH}_2]_2 \cdot \text{TiCl}_6$  was originally produced to ensure the procedure would work efficiently. Following this, the amount of  $\text{TiCl}_4$  and dimethylamine hydrochloride was calculated to produce 5 grams of product. To make 5 grams of product, 2.312 grams of dimethylamine hydrochloride was weighed out in a vial inside the nitrogen filled bag. In a separate dram vial, 2.688 grams of  $\text{TiCl}_4$  was weighed out. A volume of 12 mL of chloroform, pre-dried with molecular sieves, was measured out and added to the dimethylamine hydrochloride. The same amount of chloroform was then added to the vial containing  $\text{TiCl}_4$ . The two were shaken to dissolve the solid and mix the solution. Using a disposable glass pipette, the  $\text{TiCl}_4$  solution was slowly added drop-wise to the dimethyl amine solution, while constantly swirling the dimethyl amine. Cloudy yellow compound started to form. Once all was added, the mixture was placed on the stir plate. The mixture was stirred for 12 hours on a smaller stir plate inside the nitrogen filled bag. Paper towels were placed between the flask and stir plate to ensure heating did not occur. The stir plate

was set to low. After the 12 hours of stirring, the mixture was covered with parafilm and left to sit for a day without stirring. After 24 hours, a vacuum filtration apparatus was put inside the nitrogen bag. A pre-weighed filter was added to the filtration apparatus. Chloroform was used to wet the filter. The compound (not fully solid) was filtered and the flask was rinsed sparingly with chloroform. Once the compound looked dry, the filter paper was placed on a watch glass, removed from nitrogen bag, and quickly placed in the desiccator to further dry. Once dried, the filter paper was weighed, and the percent recovery of product was 70%. Loss of product occurred during the filtration process. The final product is shown in **Figure 4**.

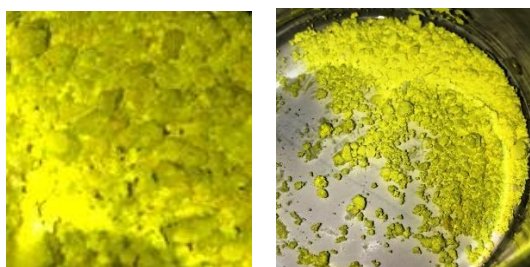


**Figure 4.** Titanium precursor,  $[(\text{CH}_3)_2\text{NH}_2]_2 \cdot \text{TiCl}_6$ , after being dried in a desiccator.

### 2.1.3 Bis(dimethylammonium) Tetrachloronickelate, $[(\text{CH}_3)_2\text{NH}_2]_2 \cdot \text{NiCl}_4$

The same procedure utilized to synthesize the bis(dimethylammonium) hexachlorotitanate was followed for the synthesis of bis(dimethylammonium) tetrachloronickelate. The synthesis of the nickel precursor, bis(dimethylammonium) tetrachloronickelate, was carried out using the following reaction:



In a dry nitrogen filled bag, 2.214 grams of anhydrous  $\text{NiCl}_2$  and 2.786 grams of  $(\text{CH}_3)_2\text{NH}_2\text{Cl}$  were weighed and independently dissolved in 20 mL of chloroform using separate reaction vessels to synthesize 5 grams of the nickel precursor. The  $\text{NiCl}_2$  solution was then added dropwise to the dimethylamine hydrochloride solution. The mixture was then stirred for ~12 hours until a precipitate formed. The resulting product was vacuum filtered, washed with dry chloroform, and dried before being stored in a desiccator. The calculated yield was 90% and was used without further purification. **Figure 5** shows the final Ni precursor product after it was fully dried in comparison to the starting compound,  $\text{NiCl}_2$ .

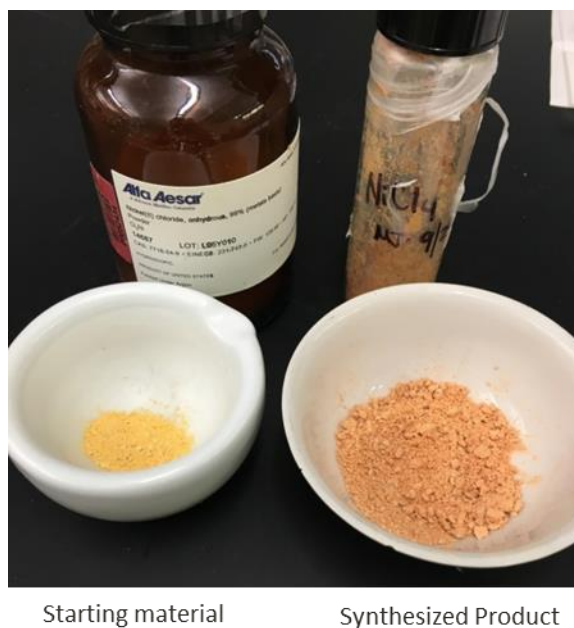
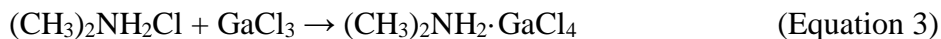


**Figure 5.** The starting  $\text{NiCl}_2$  material (left) versus the synthesized Ni precursor (right).

#### 2.1.4 Bis(dimethylammonium) Tetrachlorogallate, $[(\text{CH}_3)_2\text{NH}_2]\cdot\text{GaCl}_4$

The same synthesis procedure utilized to make the titanium and nickel precursors was followed for the synthesis of 20 grams of bis(dimethylammonium) tetrachlorogallate. The following stoichiometric reaction was used to carry out the calculations for the synthesis:



The synthesis was completed in a dry nitrogen environment. To synthesize 20 grams of the gallium precursor, 11.6 grams  $\text{GaCl}_3$  was weighed out along with 10.74 grams of  $(\text{CH}_3)_2\text{NH}_2\text{Cl}$  in two separate vessels. 150 mL of chloroform was added to the  $\text{GaCl}_3$  in a volumetric flask to dissolve the solid. The same amount was then added to the vessel containing the  $(\text{CH}_3)_2\text{NH}_2\text{Cl}$ . The flask containing the dimethylamine chloride was clamped to a ring stand and placed above a stir plate, and a stir rod was added. The solution was vigorously stirred. The gallium chloride in chloroform was then slowly added to the dimethylamine solution. While the gallium was being added, a cloud of smoke formed in the flask. This was excess chlorine gas evacuating from the solution. The solution was then stirred for 24 hours. After the 24 hours, the compound inside the flask appeared to be a bright white powdery substance. The original  $\text{GaCl}_3$  was more of a translucent, clear, crystalline solid. The flask was removed from the stir plate. Using a metal spatula, the solid product was scraped from the sides of the flask and more chloroform was added to rinse the mixture. Using vacuum filtration, the compound was dried and rinsed with chloroform. Following vacuum filtration, the compound was still slightly wet so was placed in a ceramic dish to fully dry out in a desiccator. The final dried product was a white powder, which can be seen in **Figure 6**.



**Figure 6.** The synthesized gallium precursor,  $[(\text{CH}_3)_2\text{NH}_2]\cdot\text{GaCl}_4$ .

## 2.2 Instrumental Analysis

### 2.2.1 Fourier-Transform Infrared Spectroscopy (FT-IR)

Fourier-Transform Infrared Spectroscopy (FT-IR) can be used for the identification or confirmation of production materials and can assist in allowing fine distinction between like materials. The infrared spectrum of a compound can reveal absorption bands of specific functional groups relative to the entire compound and any interactions between surrounding molecules within the compound. A FT-IR equipped with a photoacoustic detector are useful for moisture sensitive samples and solid samples that are not easily ground into a fine, even powder. FT-IR spectroscopy uses infrared radiation at an acoustical frequency when utilizing a photoacoustic detector. This radiation is absorbed by a sample, converting the radiant energy to heat. The heat causes the surrounding helium gas to expand and contract at that frequency and acoustical waves are generated and detected. The resulting signal is an interferogram, which is Fourier transformed to produce a single-beam spectrum as a function of frequency (Equation 4).<sup>41</sup>

$$P(\bar{\nu}) = \int_{-\infty}^{+\infty} P(x) \cos(2\pi x \bar{\nu}) dx \quad (\text{Equation 4})$$

Where:

$P(\bar{\nu})$  = intensity of source at frequency  $\bar{\nu}$

$P(x)$  = intensity of the total beam at the detector

$\bar{\nu}$  = frequency ( $\text{cm}^{-1}$ )

$x$  = mirror displacement (cm)

For this research, FT-IR is utilized to determine differences between the starting materials of the Ni precursor and the final product. FT-IR measurements were achieved using a Digilab FT-IR FTS-7000 spectrometer with a MTEC model 300 photoacoustic detector. The photoacoustic response was obtained using 64 scans that were averaged to produce a single spectrum with a final resolution of  $2 \text{ cm}^{-1}$ . The spectral range analyzed was from  $400$  to  $4000 \text{ cm}^{-1}$ , the mid-infrared region. The far-infrared region below  $400 \text{ cm}^{-1}$  is typically used to study organometallic complexes, specifically the metal ions of these complexes. However, this specific FT-IR spectrometer is only capable of analyses above  $400 \text{ cm}^{-1}$  because it is not equipped with the detector, optical system, or source of radiation required for far-infrared analyses. Prior to analysis all samples were thoroughly purged with helium which acted as the signal transducer.

### 2.2.2 UV/Vis Spectroscopy Analysis

UV/Vis spectroscopy is often used for the identification of various compounds based on their absorption versus wavelength in the ultra-violet/visible region of the electromagnetic spectrum. UV/Vis spectrophotometers use a beam of radiation that passes photons through molecules in a solution. Some of the photons are absorbed when they collide with molecules,

which raises the molecules to an excited state. The molecules of various compounds only absorb photons of energy in specific regions of the spectrum. The absorption spectrum that is displayed for absorption versus wavelength serves as a foundation for identification of various compounds. The absorbance in relation to the concentration of the compound is defined by the Beer-Lambert Law (Equation 5) and is a linear relationship.

$$A = -\log(T) = \epsilon bc \quad (\text{Equation 5})$$

Where:

A= Absorbance

T= Transmittance

$\epsilon$ = molar absorptivity (liter/mol/cm)

b= path length (cm)

c= concentration (mol/L)

UV/Vis spectroscopy measurements were performed using an Agilent Technologies Cary 100 UV-Vis. Data was collected between the wavelength range of 200 nm and 800 nm at 1 nm intervals. The scan rate was 600 nm/min. Samples were run in replicates of three and the spectra were averaged. The spectra of  $[(\text{CH}_3)_2\text{NH}_2]_2 \cdot \text{NiCl}_4$  and  $\text{NiCl}_2$  were overlaid to analyze the differences in absorption.

### 2.2.3 Powder X-Ray Diffraction (XRD) Analyses

Powder X-ray diffraction, or powder XRD can be used to identify the structure of solid powder compounds or crystalline phases in a material. Powder XRD works by emitting an X-ray



on a powder or crystalline substance. The X-ray is then scattered in all directions. The diffraction pattern from the X-ray beams can be described by Bragg's law (Equation 6).<sup>41</sup>

$$2d(\sin\theta) = n\lambda \quad (\text{Equation 6})$$

Where:

$d$  = lattice interplanar spacing of the crystal

$\theta$  = x-ray incidence angle (Bragg angle)

$\lambda$  = wavelength of the characteristic X-rays

$n$  = integer

A diffraction pattern of an unknown substance can be compared to diffraction patterns of known substances. If the unknown substance is made up of differing compounds, then each component must be identified separately. The only downside to this is if there is not a known substance in a database that can be matched with the unknown compound, which can make it difficult to determine the crystalline phase and structure.

Powder X-ray diffraction (XRD) analyses were accomplished using Bruker D8 ADVANCE Vario Powder X-ray Diffractometer with a primary monochromator and fast silicon strip detector.  $[(\text{CH}_3)_2\text{NH}_2]_2\cdot\text{NiCl}_4$  was finely ground using a mortar and pestle and evenly placed in a flat sample holder. The sample was run for two hours, and the angle was scanned from 10 degrees to 90 degrees. The wavelength used was 1.54 Å (Cu  $K\alpha$ ). DIFFRAC.EVA program was utilized for phase identification along with the ICDD PDF2 database. TOPAS software was exploited for indexing the compound for structure determination and Rietveld structure refinement. The Inorganic Crystal Structure Database (ICSD) was then used to obtain

the diffraction pattern for anhydrous  $\text{NiCl}_2$ . This was plotted against the diffraction pattern of  $[(\text{CH}_3)_2\text{NH}_2]_2 \cdot \text{NiCl}_4$  for comparison.

#### 2.2.4. Electrochemical Apparatus and Conditions

Potentiometry measures the electrode potential resulting from the concentration or activity of an active ion. The potential is measured relative to a reference electrode. Utilizing various potential step methods and voltammetric methods can help in the determination of the composition of several analytes and can help to control oxidation states that affect a substance's reactivity.<sup>41</sup>

This research included voltammetric methods such as linear potential sweep voltammetry and cyclic voltammetry. A CH Instruments 660C potentiostat/galvanostat with included software was used for all electrochemical experiments along with a three-electrode, one-compartment cell. The reference electrode was an Ag/AgCl electrode, with 3 M KCl filling solution. The counter electrode was a platinum sheet with immersed surface area  $\sim 2$  times greater than the working electrode. The working electrode used was a grafoil sheet electrode (Graftech, Grafoil flexible Graphite GTA) with electrochemical area =  $1.2 \text{ cm}^2$ . A Ni disc electrode (3 mm diameter, area =  $7.07 \times 10^{-2} \text{ cm}^2$ ) was used as an electrochemical standard for comparison to the PANI/Ni composite. A scan rate of 10 mV/s was used for all experiments. All experiments were carried out in ambient room temperature.

#### 2.2.5 Scanning Electron Microscopy (SEM)/Energy Dispersive Spectroscopy (EDS)

A scanning electron microscope (SEM) allows for the nondestructive elemental analysis of a solid sample. An SEM uses an electron gun to direct a beam of electrons at a sample. The electron bombardment then excites X-rays in the sample.<sup>41</sup> The microscope allows for the continuous observation of the sample. The beam of electrons only penetrates a very small area,

which makes it ideal for thin layer samples. Energy dispersive spectroscopy or energy dispersive X-ray analysis is often used in conjunction with SEM. Energy dispersive detectors can differentiate between various elements and their X-ray lines, and their intensities can be relative to the elemental concentrations.<sup>41</sup>

SEM images were obtained using JEOL JSM-5610 Scanning Electron Microscope equipped with a secondary electron (SEI) detector and Backscattered electron detector (BEI) and an Oxford ISIS EDS system with a low noise Integrated Transistor Reset Preamplifier (I-TRP), capable of qualitative, pseudo-quantitative analyses, and x-ray mapping. The composites were attached to the sample holder with carbon tape and measurements were performed at 20 kV with a working distance of 26 mm. A JEOL JSM-6700F Field Emission Scanning Electron Microscope (FESEM) equipped with a secondary electron detector (SEI) was also utilized for analyzing the composites. The magnification range is x500 to x430,000 with a resolution of 10 nm. The imaging conditions were 8 kV with a working distance of 7.6 mm and magnification of x20,000. The composites were also analyzed by energy dispersive X-ray (EDX/EDS).

## Chapter 3. Characterization and Electrochemical Analysis of PANI/Ni Composites

### 3.1 Introduction

This chapter summarizes the characterization of the synthesized Ni precursors. FT-IR spectroscopy, UV/Vis spectroscopy, and powder XRD are utilized to characterize the Ni precursors. FT-IR spectroscopy allows for the comparison of various functional groups that make up the Ni precursors and those of the starting components. UV/Vis spectroscopy assists in further verifying the structure of the Ni precursors in comparison to the starting component  $\text{NiCl}_2$ . Powder XRD provides a diffraction pattern of the Ni precursor that can be used in comparison to  $\text{NiCl}_2$  to further differentiate the Ni precursor from its starting components. Following characterization, Ni on grafoil and PANI/Ni composites are formed electrochemically by linear scan voltammetry. Both the Grafoil/Ni and PANI/Ni composites are verified using SEM/EDS analyses. Finally, the oxidant properties and catalytic activity of the composites are analyzed in KOH and 1 M  $\text{CH}_3\text{OH}/\text{KOH}$ , respectively, using cyclic voltammetry.

### 3.2 Characterization of Ni Precursors

#### 3.2.1 FTIR Spectroscopy of Ni Precursors

The photoacoustic FTIR spectra in the region encompassing 500 and 4000  $\text{cm}^{-1}$  was obtained for the reactants ( $\text{NiCl}_2$  and  $(\text{CH}_3)_2\text{NH}_2\text{Cl}$ ) and the Ni precursor product ( $[(\text{CH}_3)_2\text{NH}_2]_2 \cdot \text{NiCl}_4$ ), **Figure 7**. The vibration bands that are associated with each absorption frequency from the FTIR spectra are listed and compared to a similar compound containing an ethylenediammonium cation and  $\text{NiCl}_4^{2-}$  anion (**Table 1**).<sup>42</sup> The  $\text{NiCl}_2$  starting material is provided in **Figure 7a**. The spectrum for  $\text{NiCl}_2$  contains absorbance bands located at 3400–3500  $\text{cm}^{-1}$  and 1605  $\text{cm}^{-1}$ , which are consistent with contamination from water and formation of either NiO or  $\text{Ni}(\text{OH})_2$ .<sup>43-44</sup>

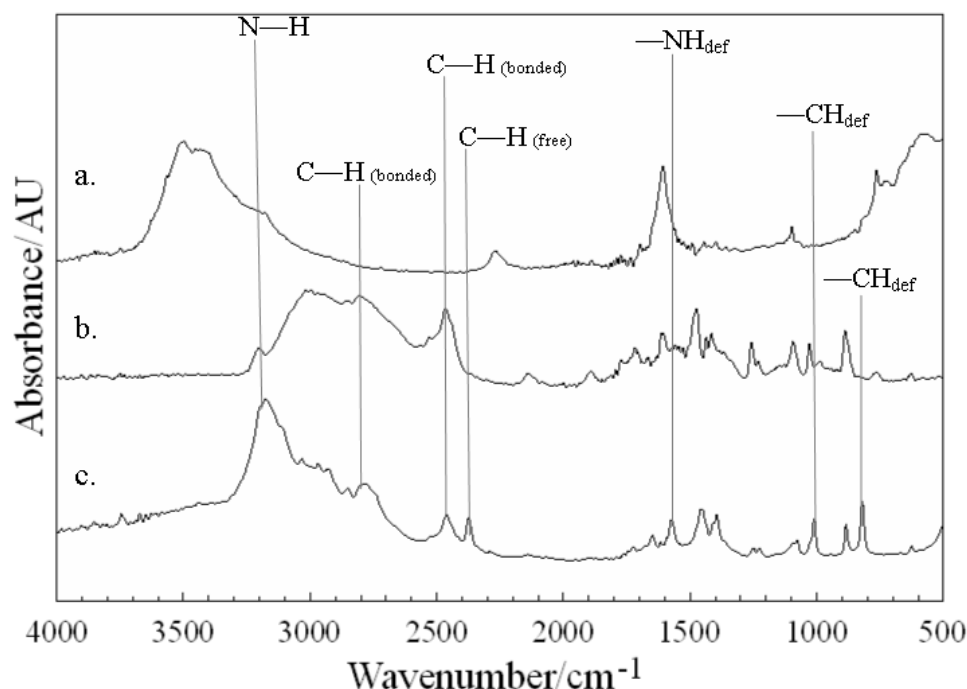


**Figure 7.** FTIR photoacoustic response of the starting components (a)  $\text{NiCl}_2$  and (b)  $(\text{CH}_3)_2\text{NH}_2\text{Cl}$ , and of the synthesized (c) Ni Precursor,  $[(\text{CH}_3)_2\text{NH}_2]_2 \cdot \text{NiCl}_4$ .

**Table 1.** Far-Infrared Absorption Frequencies ( $\text{cm}^{-1}$ ) obtained for the starting compounds and for the Ni precursor.

Table 1. Far-Infrared Absorption Frequencies ( $\text{cm}^{-1}$ )									
Band	—OH	N—H	C—H Bonded	C—H Free*	H—O—H	NH def*	—CH <sub>3</sub>	C—N	—CH def*
(a.) $\text{NiCl}_2$	3400-3500				1607				
(b.) $(\text{CH}_3)_2\text{NH}_2\text{Cl}$		3200	2465, 2700-3000				1231, 1258, 1416, 1437,	889, 1028	
(c.) $[(\text{CH}_3)_2\text{NH}_2]_2 \cdot \text{NiCl}_4$		3175	2461, 2700-3000	2374		1011, 1574	1227, 1250, 1395, 1408, 1458	885, 1024	820
$[\text{NH}_3\text{CH}_2\text{CH}_2\text{NH}_3] \cdot \text{NiCl}_4$ <sup>40</sup>						1013, 1574		1059	784

\* Specific for  $\text{NiCl}_4^{2-}$  anion.

<sup>41</sup> Ba.S. Skaarup, R.W. Berg, Structural Properties and Vibrational Spectra of Ethylenediammonium Family of Perovskite Layer-type Crystals -  $\text{NH}_3\text{CH}_2\text{CH}_2\text{NH}_3 \text{MCl}_4$ ,  $\text{M}=\text{Ni}$ ,  $\text{Pd}$ ,  $\text{Cu}$ ,  $\text{Cd}$ ,  $\text{Mn}$ , *J. Solid State Chem.*, 26 (1978) 59-67. FTIR data obtained from 100  $\text{cm}^{-1}$  to 1600  $\text{cm}^{-1}$ .

The  $\text{NiCl}_2$  does not traditionally have absorbance bands at these energies. In contrast, there are several absorption bands that are similar for  $(\text{CH}_3)_2\text{NH}_2\text{Cl}$  and the Ni precursor, **Figure 7b** and **7c**. These bands are characteristic of the C—H (bonded) stretch of the methyl groups, N—H stretch of the amine groups, — $\text{CH}_3$  rotations, and the C—N stretch of the starting component and the cation of the Ni precursor.

For the Ni precursor, the band at  $2461\text{ cm}^{-1}$  and at  $2793\text{ cm}^{-1}$  for the C—H (bonded) stretch appears much broader and more intense than the band for  $(\text{CH}_3)_2\text{NH}_2\text{Cl}$ , **Figure 7b** and **7c**. There are no publications that provide IR frequencies for this specific Ni anion complex. However, articles have been published for other halide salt complexes that show this band is consistent with C—H - -Cl hydrogen bonding from the  $\text{NiCl}_4^{2-}$  anion to the hydrogen of the methyl group in the  $((\text{CH}_3)_2\text{NH}_2)^{2+}$  cation.<sup>45-46</sup> A sharp singlet peak is observed for the Ni precursor at  $2374\text{ cm}^{-1}$  with an additional band at  $2793\text{ cm}^{-1}$ , These bands have been previously identified for similar halide salt complexes due to C—H (free) stretching vibrations that come from the hydrogen of the methyl group that are not involved in hydrogen bonding with the anion of the precursor.<sup>46-47</sup> This leads to the speculation that the geometry of the anion about a methyl group of the alkylammonium cation is tetragonal. Slight shifting and increases in absorption for N—H stretching region, the C—N stretching region and the — $\text{CH}_3$  bends observed for the Ni precursor in comparison to  $(\text{CH}_3)_2\text{NH}_2\text{Cl}$  are due to the interaction of the anion and cation of the metal precursor.<sup>45-52</sup> The —NH deformation at  $1011\text{ cm}^{-1}$  and  $1574\text{ cm}^{-1}$  are very comparable to previously published data for  $\text{NiCl}_4^{2-}$  with an ethylene diammonium cation, which reported —NH deformation at  $1013\text{ cm}^{-1}$  and  $1574\text{ cm}^{-1}$ .<sup>42</sup> The band for  $[(\text{CH}_3)_2\text{NH}_2]_2\cdot\text{NiCl}_4$  at  $820\text{ cm}^{-1}$  is associated with —CH deformation. In comparison to the similar compound  $[\text{NH}_3\text{CH}_2\text{CH}_2\text{NH}_3]\cdot\text{NiCl}_4$ , —CH deformation was recorded at  $784\text{ cm}^{-1}$  and was claimed to be

from the *trans*-cation conformation to the metal halide anion, but the actual wavelength can vary based on the interacting cation.<sup>42, 53-54</sup> The Ni precursor shows photoacoustic responses similar to the  $(\text{CH}_3)_2\text{NH}_2\text{Cl}$  reactant and to other alkylammonium tetrachloronickelate complexes, but because no literature can be found for this specific Ni precursor, further analysis is required to confirm the structural aspects of this compound.

### 3.2.2 UV/Vis Spectroscopy of Ni Precursors

Initially, two aqueous solutions containing 50 mM of  $\text{NiCl}_2$  and dimethylamine tetrachloronickelate  $[(\text{CH}_3)_2\text{NH}_2]_2\cdot\text{NiCl}_4$  (nickel precursor) were prepared and analyzed to determine if there were significant differences in the spectroscopic properties. The corresponding spectra for each species are presented in **Figure 8**.

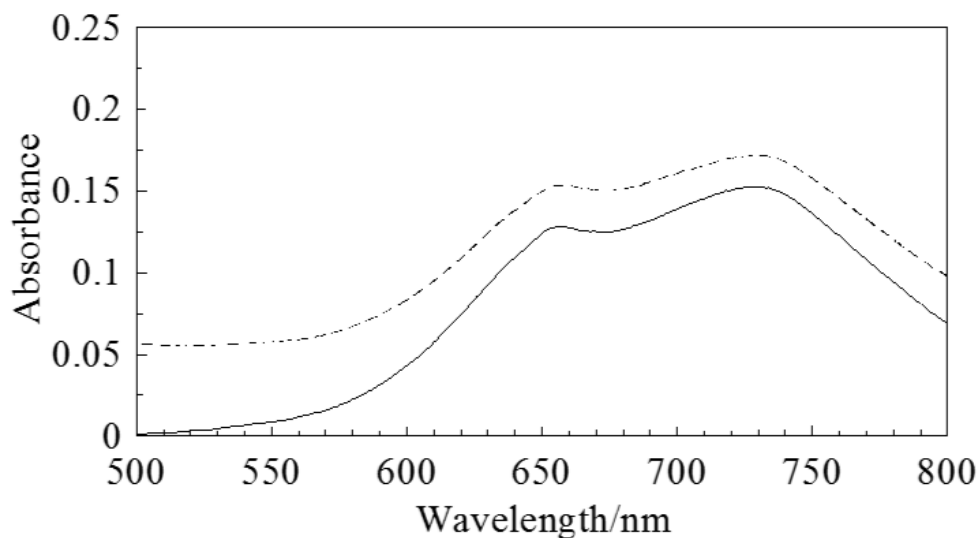


**Figure 8.** UV/Vis absorbance spectrum for 50 mM  $\text{NiCl}_4^{2-}$  (solid line) and 50 mM  $\text{NiCl}_2$  (dashed line) in  $\text{H}_2\text{O}$ .

The spectra for  $\text{NiCl}_2$  (dashed line) and the nickel precursor (solid line) are very similar with absorption bands at  $\lambda_{\text{max}} = 656 \text{ nm}$  and  $723 \text{ nm}$ . The data suggests that there is little difference between the starting material and the product. However, previous studies have shown that both nickel chloride complexes can interact with water, a protic solvent, to form aquo-complexes with similar absorbance bands in the spectral region between 550 to 800 nm.<sup>55-56</sup> In contrast, ionic liquid, an aprotic solvent, has little to no water content and can be further dried with molecular sieves.<sup>57</sup> Therefore, ionic liquid was utilized to obtain more useful information about the spectral characteristics of  $\text{NiCl}_2$  and the Ni precursor. For comparison, 50 mM solutions of both the nickel dichloride and the nickel precursor were prepared in ionic liquid N,N,N-trimethyl-N-butylammonium bis(trifluoromethanesulfonyl)imide (IL). The goal was to eliminate any conversion of the chloride complexes in water, which would resolve any spectral differences between the two materials.<sup>55, 58</sup> The UV/Vis spectra for the two species dissolved in IL are provided in **Figure 9**.

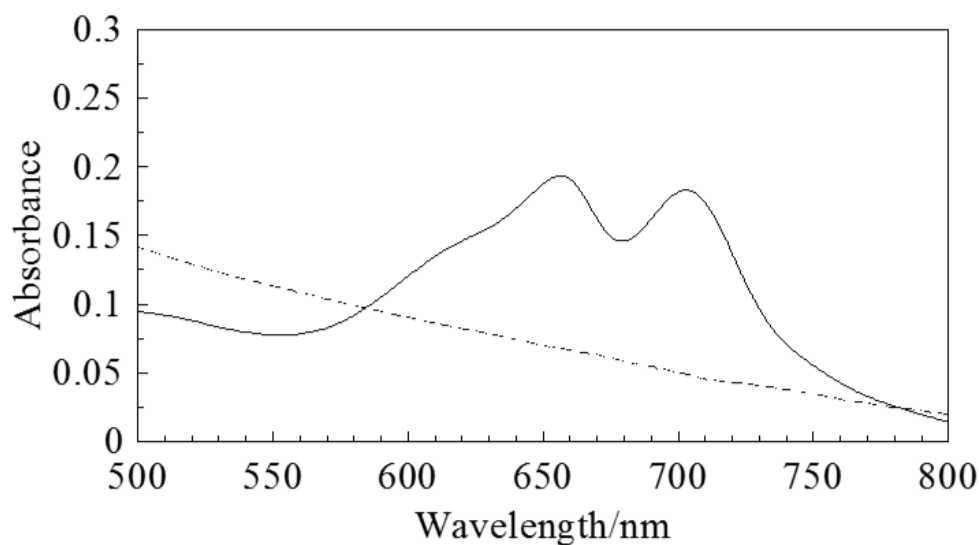


**Figure 9.** UV/Vis absorbance spectra for 50 mM  $\text{NiCl}_4^{2-}$  (solid line) and 50mM  $\text{NiCl}_2$  (dashed line) in ionic liquid.



The response for nickel dichloride (dashed line) does not have absorbance bands in the spectral region between 500 – 800 nm that were observed in aqueous solution. In contrast, the nickel precursor (solid line) has multiple absorbance bands at  $\lambda_{\text{max}} = 655 \text{ nm}$  and  $703 \text{ nm}$ . These bands have been previously assigned to the tetrahedral  $\text{NiCl}_4^{2-}$  complex anion, which are due to transitions from the  ${}^3\text{T}_1(\text{F})$  state to the  ${}^3\text{T}_1(\text{P})$  state.<sup>55-61</sup> Therefore, the spectral data is consistent with the formation of the nickel precursor  $\text{NiCl}_4^{2-}$ .

### 3.2.3 Powder X-Ray Diffraction of Ni Precursors

FTIR spectroscopy and UV/Vis spectroscopy provided useful information about the relative composition of the Ni precursors. However, these spectroscopic methods did not provide any information about the crystal structure and unit cell dimensions. Therefore, the Ni precursors were analyzed by powder XRD to gain further insight into the structure of the synthesized precursors (**Figure 10**).

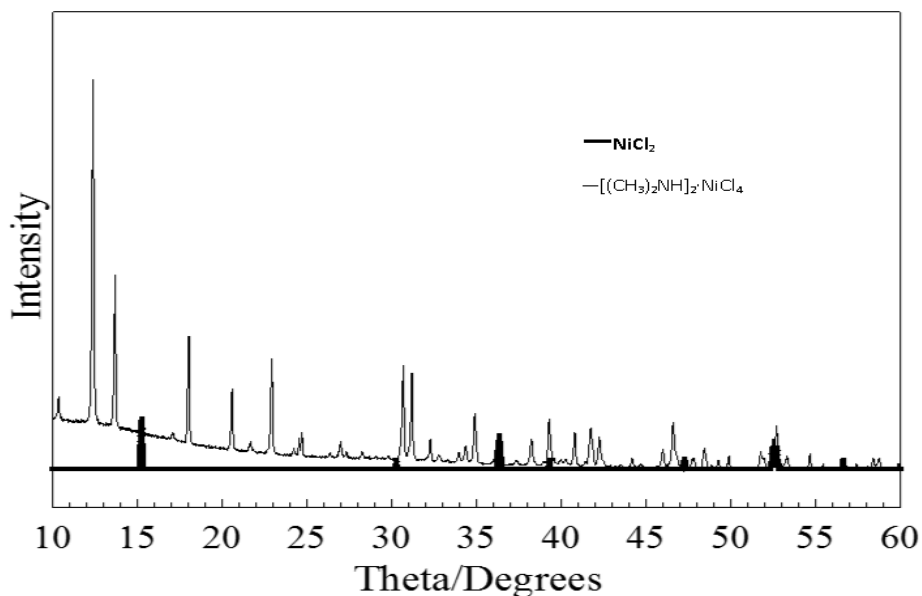


**Figure 10.** Powder XRD of Ni Precursor,  $[(\text{CH}_3)_2\text{NH}]_2 \cdot \text{NiCl}_4$ , in comparison to powder XRD of the starting Ni component,  $\text{NiCl}_2$ .

Powder XRD rather than single crystal XRD was utilized because no single crystals of  $[(\text{CH}_3)_2\text{NH}_2]_2\cdot\text{NiCl}_4$  could be formed. Previously, powder XRD analyses on tetrahedral nickel complexes with disassociated cation have been determined to have a unit cell of  $D_{4h}^{7,46}$ . Similarities between the  $\text{NiCl}_2$  starting material and the Ni precursor occur around  $2\theta = 36, 39, 52,$  and  $53$  degrees. Several different peaks are visible for the Ni precursor, which show that the crystal structure is very different from the  $\text{NiCl}_2$  starting material. This further indicates that the Ni precursor was synthesized correctly.

### 3.3 Electrochemical Synthesis of Ni Composites

#### 3.3.1 Ni Electrochemistry on Grafoil

The deposition of Ni using  $\text{NiCl}_4^{2-}$  was evaluated using an aqueous solution containing 50 mM  $[(\text{CH}_3)_2\text{NH}_2]_2\cdot\text{NiCl}_4$ . Linear Scan Voltammetry (LSV) data for a grafoil electrode immersed in the solution containing the nickel precursor is provided in **Figure 11**. The figure shows five successive reduction scans for the grafoil electrode in the 50 mM  $\text{NiCl}_4^{2-}$  solution. The electrochemical reduction of the Ni precursor was initiated by holding the grafoil electrode at 1 V. The cathodic scan was initiated after two minutes and terminated at -0.2 V. The reduction of  $\text{NiCl}_4^{2-}$  is not resolved for the first voltammetric scan. However, two voltammetric waves are resolved for the second reduction cycle, which appear at  $\sim 0.7$  V and  $\sim 0.45$  V. In addition, the two voltammetric waves continue to increase with each successive voltammetric scan. The increase in current as a function of reduction cycles is consistent with increasing Ni content at grafoil.

The two reduction waves observed in the voltammetry are not easily assigned because there is a lack of data regarding the electrochemical reduction of  $\text{NiCl}_4^{2-}$ . In addition, the formation of Ni oxide is possible at 0.8 V in the Ni precursor solution. Therefore, the

voltammetric waves are likely consistent with the reduction of the Ni precursor and possible formation of Ni oxide. Further studies are required to determine the exact mechanism for Ni deposition at the grafoil electrode using the Ni precursor.

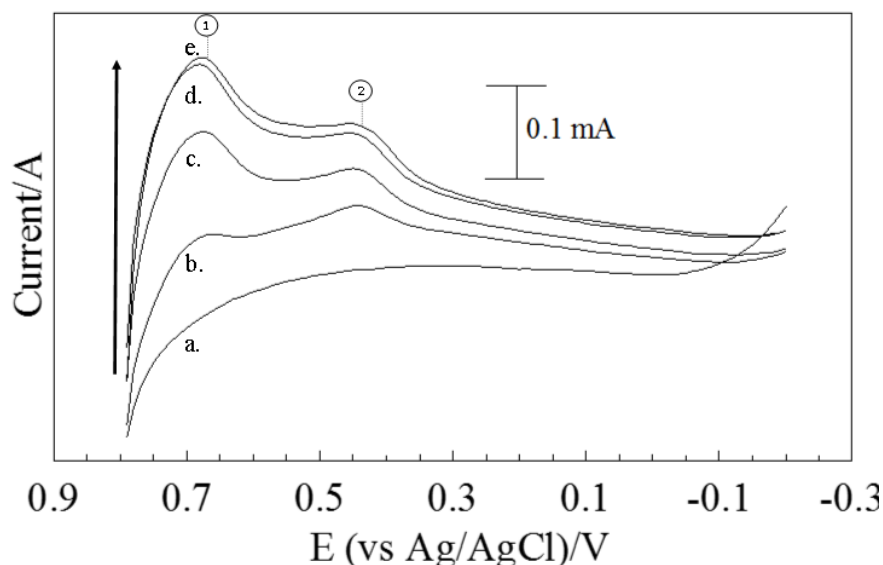


**Figure 11.** Sweep-step function voltammetric response of (a) first step scan of 50 mM  $\text{NiCl}_4^{2-}$  deposited on grafoil, (b) second step scan of 50 mM  $\text{NiCl}_4^{2-}$  deposited on grafoil (c) third step scan of 50 mM  $\text{NiCl}_4^{2-}$  deposited on grafoil, (d) fourth step scan of 50 mM  $\text{NiCl}_4^{2-}$  deposited on grafoil, (e) fifth step scan of 50 mM  $\text{NiCl}_4^{2-}$  deposited on grafoil. The scan rate is 10 mV/s.

### 3.3.2 SEM/EDX Ni on Grafoil

SEM analysis was used to evaluate the morphology of deposits on grafoil using the Ni precursor. The SEM images of grafoil before Ni deposition and after five sweep-step depositions of 50 mM  $\text{NiCl}_4^{2-}$  are shown in the **Figure 12a** and **12b**, respectively. The Ni deposits uniformly cover the grafoil surface with additional smaller islands on the surface. The size of the Ni deposits on the surface is approximately 5  $\mu\text{m}$  with additional deposits that are smaller. Cracking was also visible for the Ni deposits, which is consistent with the deposition of thick Ni oxide.<sup>62</sup> EDX analyses identified Ni at 0.8 KeV, 7.5 KeV, and 8.3 KeV. Oxygen peaks were

visible at 0.5 KeV and Cl appeared at 2.6 KeV. The response from oxygen is consistent with the formation of nickel oxide when exposed to atmosphere. The Ni deposits were not excessively washed to ensure the NiO film was not destroyed. Therefore, there is residual Cl observed, which is attributed to excess chloride ion from the reduction of the Ni precursor. In addition, there is a strong carbon signal observed, which is consistent with the grafoil electrode. The data implies that the Ni deposits are porous and the grafoil electrode is not fully covered. The SEM data confirm that the electrochemical reduction of Ni precursor resulted in the deposition of NiO onto the grafoil.

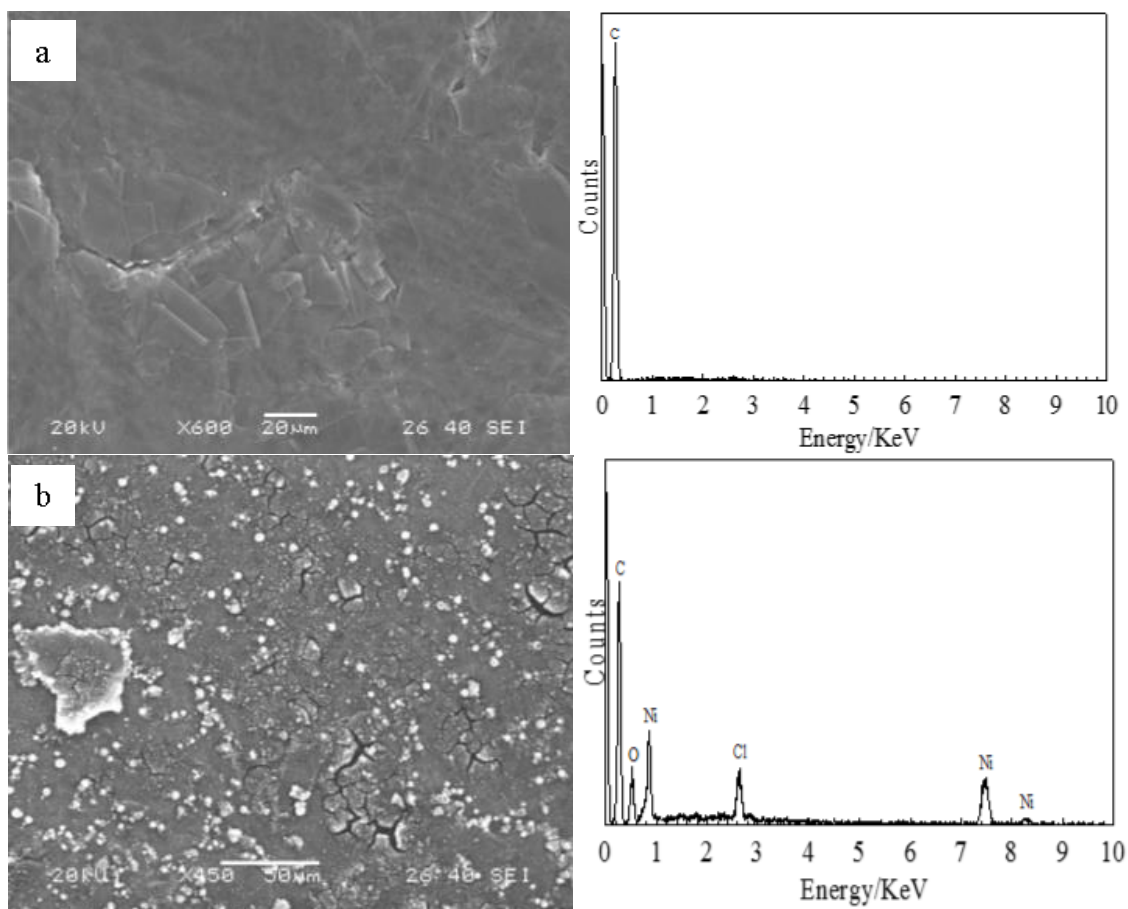
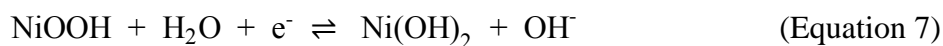


**Figure 12.** SEM image and EDX data of (a) grafoil (x600, 20kV) and (b) 5 sweep step depositions of 50 mM NiCl<sub>4</sub><sup>2-</sup> on grafoil (x450, 20kV).

### 3.3.3 Grafoil/Ni Electrochemistry in KOH

After each successive deposition of the Ni precursor, the grafoil electrode was examined electrochemically in 1 M KOH (pH 14.0). For comparison, the cyclic voltammetric responses for a Ni disc electrode immersed in 1 M KOH is presented in **Figure 13a**. The cathodic scan for the Ni electrode shows a reduction peak at 0.35 V. The reverse anodic scan has an oxidation peak at 0.50 V. There are no other oxidation/reduction processes that are resolved for the Ni disc electrode. The redox couple observed in the cyclic voltammetry has been previously attributed to the following chemical reaction:<sup>63-66</sup>



The oxidation of Ni has been previously observed between 0.45 V and 0.55 V in basic solutions. However, the reduction peak usually occurs between 0.54 V and 0.37 mV, which is consistent with the data provided in **Figure 13**.<sup>63, 66</sup> The cyclic voltammetric response of a grafoil electrode in 1M KOH prior to Ni precursor reduction is provided in **Figure 13b**. There is no visible oxidation/reduction for grafoil in the potential range observed for the Ni electrode. Finally, the cyclic voltammetric response for grafoil after the first and fifth reduction of Ni precursor is provided in **Figure 13c**. The cathodic scan for the first sweep-step deposition of Ni precursor (dotted line) shows a reduction peak at 0.25 V. The reverse anodic scan has an oxidation peak at ~0.37 V. After five sweep-step depositions of Ni precursor (solid line), the cathodic scan shows a reduction peak at 0.30 V, and the reverse anodic scan shows an oxidation peak at 0.40 V. The increase in current and steady shift of the redox couple to more positive potentials with each successive deposition of Ni precursor is consistent with increasing Ni oxide film at grafoil.<sup>64</sup> A second oxidation peak for the first deposition and fifth deposition of Ni

precursor is visible at -0.50 V and 0 V, respectively. Although the oxidation peak is visible in previous studies, there has been no clear explanation of the nickel species that give rise to the voltammetric wave.<sup>63-67</sup> Water oxidation is also visible when the applied potential exceeds 0.70 V for both the first sweep-step and fifth sweep-step deposition of Ni precursor. The voltammetry is consistent with NiO surface, which exhibits high stability and performance for water oxidation.<sup>68</sup> In addition, previous research has shown that amorphous NiOOH can contribute to water oxidation.<sup>68-71</sup>

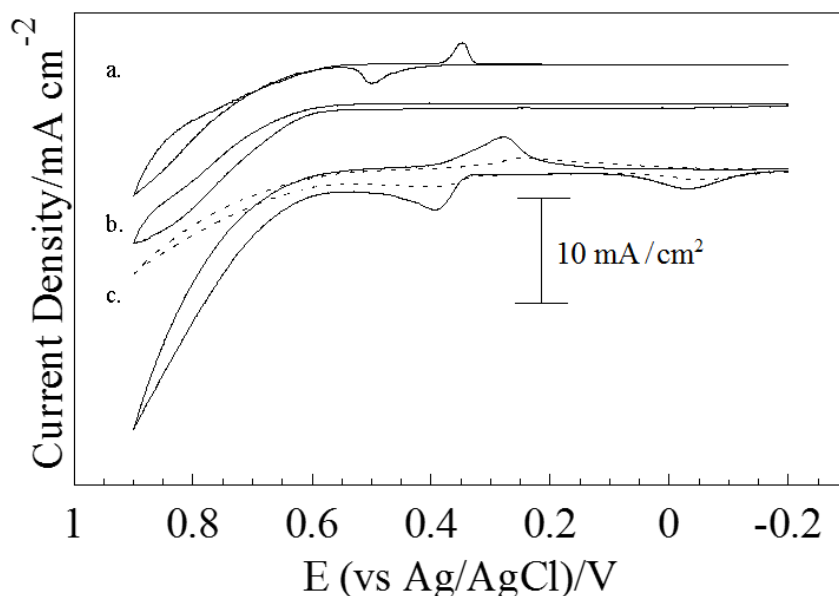


**Figure 13.** Steady-state cyclic voltammetric response of (a) Ni disc electrode (3mm), (b) response of Grafoil electrode (c) response of Grafoil/1 Ni and Grafoil/5 Ni after the 10<sup>th</sup> voltammetric scan in solution containing 1 M KOH. The largest oxidation/reduction peaks come from the 5 sweep steps of 50 mM NiCl<sub>4</sub><sup>2-</sup> on Grafoil. The smallest oxidation/ reduction peaks come from the 1 sweep step of 50 mM NiCl<sub>4</sub><sup>2-</sup> on Grafoil. The scan rate is 10mV/s.

### 3.3.4 Grafoil/Ni Electrochemistry in CH<sub>3</sub>OH/KOH

The catalytic activity of the grafoil/Ni deposit electrode was analyzed in a solution containing 1 M CH<sub>3</sub>OH/KOH. For comparison, the cyclic voltammetric responses for a Ni disc electrode immersed in 1 M CH<sub>3</sub>OH/KOH is presented in **Figure 14a**. The forward (anodic) and reverse (cathodic) scans have an oxidation peak at 0.60 V. The oxidation peaks for the forward and reverse scans coincides with the oxidation of methanol.<sup>72</sup> Similarly, the reverse (cathodic) potential sweep shows the anodic peak at 0.60 V for the oxidation of methanol and a small cathodic peak around 0.350 V. The cathodic peak has been assigned previously to the reduction of nickel oxyhydroxide to form surface adsorbed hydroxyl groups.<sup>72</sup> Hysteresis is also visible around 0.375 V, which is consistent with previous results.<sup>72-73</sup> For comparison, the voltammetric response of grafoil in 1 M CH<sub>3</sub>OH/KOH prior to nickel deposition is shown in **Figure 14b**. There is no visible oxidation/reduction for grafoil in 1 M CH<sub>3</sub>OH/KOH. The cyclic voltammetric response for a grafoil electrode after the first, third, and fifth reduction of Ni precursor is provided in **Figures 14c, d, and e**. The voltammetry is consistent for all three samples, which show the oxidation of methanol on the forward and reverse scans at ~0.65 V. The oxidation of methanol by the Ni precursor on grafoil is much greater than the oxidation of methanol by the Ni disc electrode in **Figure 14a**. A large change in current is visible from the first reduction sweep of Ni precursor to the fifth reduction sweep for the oxidation of methanol. This indicates that the oxidation of methanol increases as more Ni precursor is deposited. From the third reduction sweep to the fifth reduction sweep of Ni precursor, the change in current is much smaller, but the current for the oxidation of methanol is higher for the fifth deposition of Ni precursor. The smaller change in current could be due to the deposition of the Ni on Ni. Increased aggregation of Ni decreases the effective surface area of the electrode for catalysis.<sup>74</sup>

For the first, third, and fifth depositions of Ni precursor, water oxidation is also increasingly visible above 0.750 V, which is consistent with the NiO electrochemistry previously shown in **Figure 13**. As more Ni is deposited on the grafoil surface, the electrochemical behavior of water oxidation competes with the electro-oxidation of methanol, which is visible in **Figures 14d** and **14e**. This makes it difficult to determine the efficiency of the oxidation of methanol as the two processes overlap.

Finally, for **Figures 14c-e**, the reverse cathodic scan shows the oxidation of methanol at the same potential as the forward anodic scan, with varying current intensities. Following this, a cathodic peak appears at 0.325 V. There is a small increase in current for this cathodic peak with increasing Ni deposition. Previous research has shown the reduction of NiOOH to occur at potentials greater than 0.306 V, which is consistent with the data provided.<sup>65, 72-73</sup> The cyclic voltammetry suggests that the formation of Ni(OH)<sub>2</sub> from the reduction of NiOOH occurs on the outermost thin surface layer rather than each of the deposited layers of Ni. The data confirms the deposition of NiO at grafoil and the oxidation of methanol on the oxidized surface of nickel.



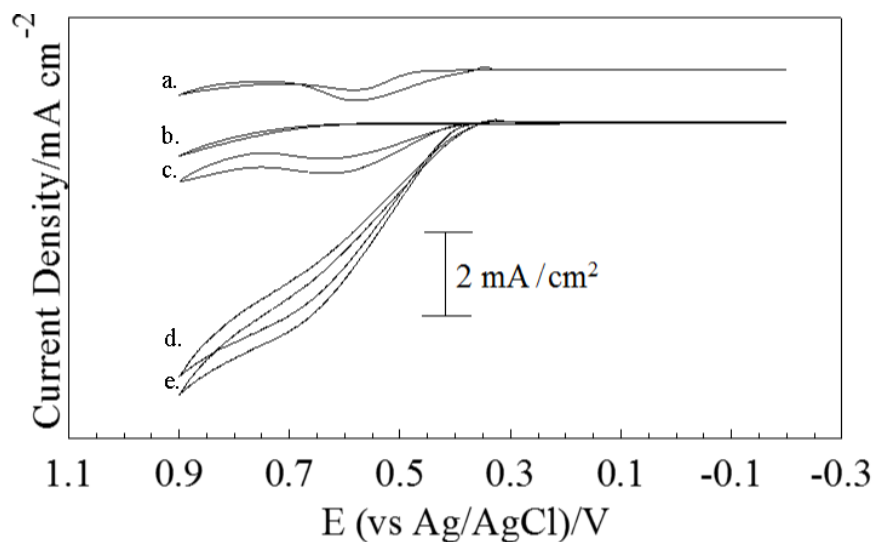


**Figure 14.** Steady-state cyclic voltammetric response of (a) Ni disc electrode (3mm), (b) Grafoil electrode (c) Grafoil/1 Ni (d) Grafoil/3 Ni, and (e) Grafoil/5 Ni after the sixteenth voltammetric scan in solutions containing 1 M KOH and 1 M CH<sub>3</sub>OH. The scan rate is 10mV/s.

### 3.4 Electrochemical Analysis of PANI/Ni Composites

#### 3.4.1 Electrochemical Synthesis of PANI

PANI films were electrochemically grown on grafoil electrodes in a solution containing 1 M perchloric acid (HClO<sub>4</sub>) and 0.25 M aniline. A single grafoil/PANI electrode was used for each electrochemical experiment to ensure the electrochemically active surface area remained constant for each experiment. Cyclic voltammetry was utilized to grow PANI on the grafoil electrode. The grafoil was cycled in the solution for 20 segments from 0.9 V to -0.2 V at a scan rate of 0.01 V/s. The starting potential was 0.5 V and the initial scan direction was positive, which allows for the oxidation of aniline to form PANI. Subsequent scans create a three-dimensional surface of polyaniline on grafoil. **Figure 15** shows the growth of PANI on grafoil, where the dotted line represents the first scan and the solid line represents the twentieth scan. Under these specific parameters, the oxidation of the aniline monomer occurred at potentials above 0.75 V (**Figure 15, A**). During the oxidation of aniline, an uptake of anions occurred. As

the potential switched and went from positive potentials to more negative potentials, anions were expelled (**Figure 15, A'**). At **Figure 15, B**, proton uptake occurred followed by proton expulsion at **B'**. The increase in current is relative to the increase in thickness of the pristine PANI.

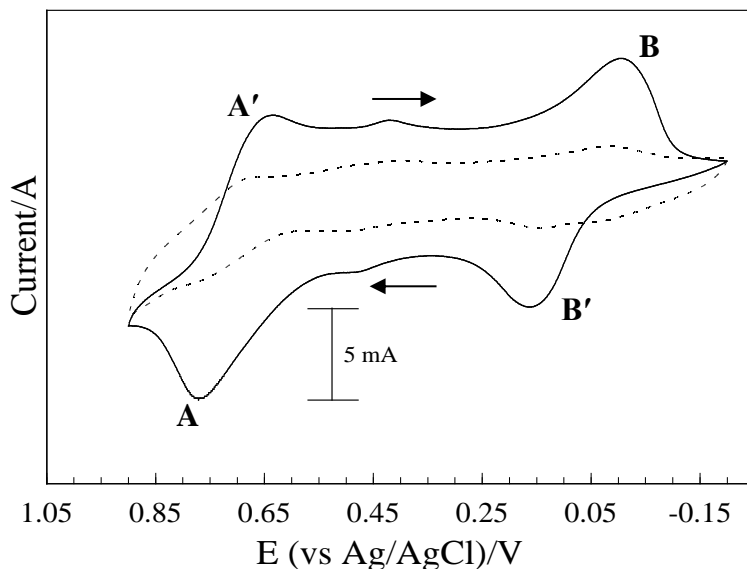


**Figure 15.** Steady-state cyclic voltammetric response of PANI growth on grafoil (working area=1.2 cm<sup>2</sup>) after the first (dotted line) and twentieth (solid line) scan; scan rate is 10 mV/s.

### 3.4.2 Ni Deposition in PANI

The grafoil/PANI electrode was immersed in 50 mM [(CH<sub>3</sub>)<sub>2</sub>NH<sub>2</sub>]<sub>2</sub>·NiCl<sub>4</sub> aqueous solution, and Linear Scan Voltammetry (LSV) was utilized for the deposition of Ni, **Figure 16**. The first, third, and fifth successive linear cathodic scans are shown for the PANI electrode immersed in the Ni precursor solution. The parameters utilized for Ni deposition in PANI were consistent with those utilized for deposition on grafoil. For each scan, the reduction of the Ni precursor is visible with two cathodic peaks at approximately 0.4 V and at 0.10 V. Although the two voltammetric waves are unresolved, they are consistent with the previous deposition of Ni at grafoil. However, the voltammetry is shifted to more negative potentials for the reduction of Ni

in PANI. With each subsequent reduction of Ni, the current decreases until it reaches steady-state by the fifth deposition. The voltammetry implies that the deposition of Ni in PANI has been achieved. To further verify the deposition and specific deposition sites on the polymer, the PANI/Ni composite will be analyzed by proton dope analyses in 1 M HClO<sub>4</sub>.

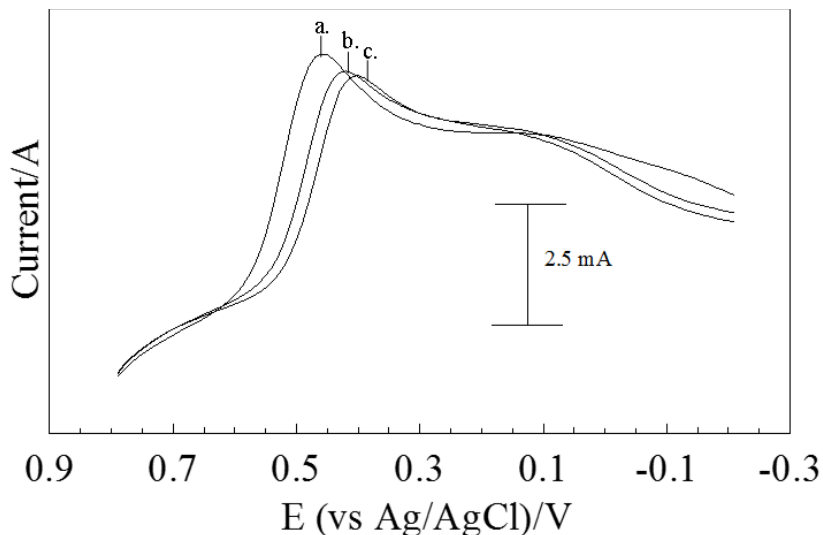


**Figure 16.** Sweep-step function voltammetric response of (a) first step scan of 50 mM NiCl<sub>4</sub><sup>2-</sup> deposited on PANI, (b) third step scan of 50 mM NiCl<sub>4</sub><sup>2-</sup> deposited on PANI, and (c) fifth step scan of 50 mM NiCl<sub>4</sub><sup>2-</sup> deposited on PANI. The scan rate is 10 mV/s.

### 3.4.3 Proton Dope Analysis of PANI/Ni Composite

Proton doping of the polymer was performed following the growth on grafoil and after Ni reduction in the polymer. The proton doping experiment was run on the electrode to verify the deposition of Ni at the nitrogen sites of the polymer. To perform the proton dope, the electrode was cycled for ten full scans in 1 M HClO<sub>4</sub> and the redox processes were analyzed. The cyclic voltammograms of each proton dope were plotted for comparison, **Figure 17**. The proton dope following PANI growth is given in **Figure 17a**. The oxidation/reduction peaks for the proton expulsion and uptake occur at 0.25 V and -0.1 V, respectively. The anion expulsion and uptake

occur at 0.76 V and 0.46 V, respectively. After five reduction steps of Ni in PANI, the peaks for the proton expulsion and uptake show very little change in potential, **Figure 17b**. However, for the peaks for the uptake and expulsion of anions, there is a noticeable shift to more negative potentials for the oxidation/reduction processes. The negative shift in potential occurs as Ni content in the polymer increases. This shift in potential is most likely due to a change in energetics associated with the oxidation of the polymer and anion uptake, which forces the anions to diffuse further in the polymer and require more energy for redox processes to occur at the nitrogen sites. Precursor deposits can interact directly with the polymer, which can then reduce anion interaction with positively charged nitrogen groups on the polymer. The shift in potential and the overall decrease in current combined with the reduction in charge associated with doping indicates that Ni deposition directly influences the oxidation/reduction of the nitrogen groups within the polymer. Therefore, Ni successfully reduced in the polymer to form PANI/Ni composites. SEM imaging and EDX analyses of the PANI/Ni composite are necessary to verify the reduction sites of Ni in PANI.

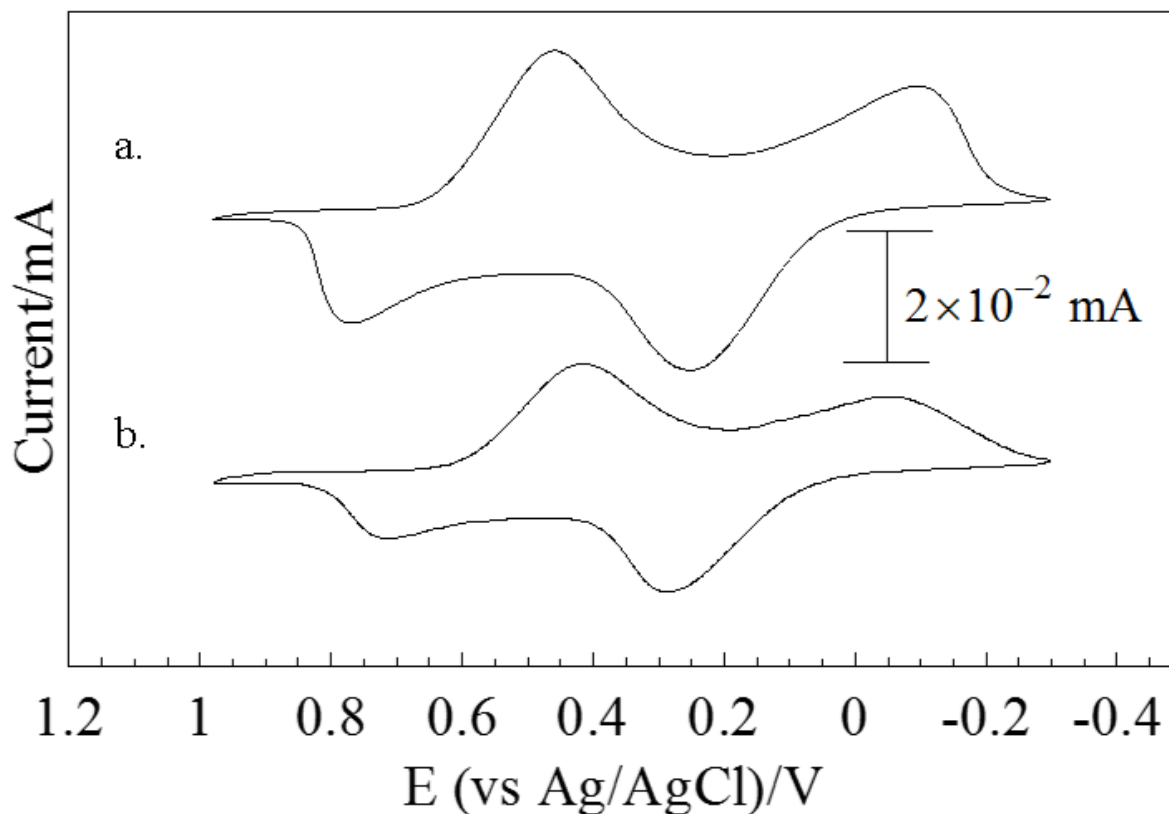
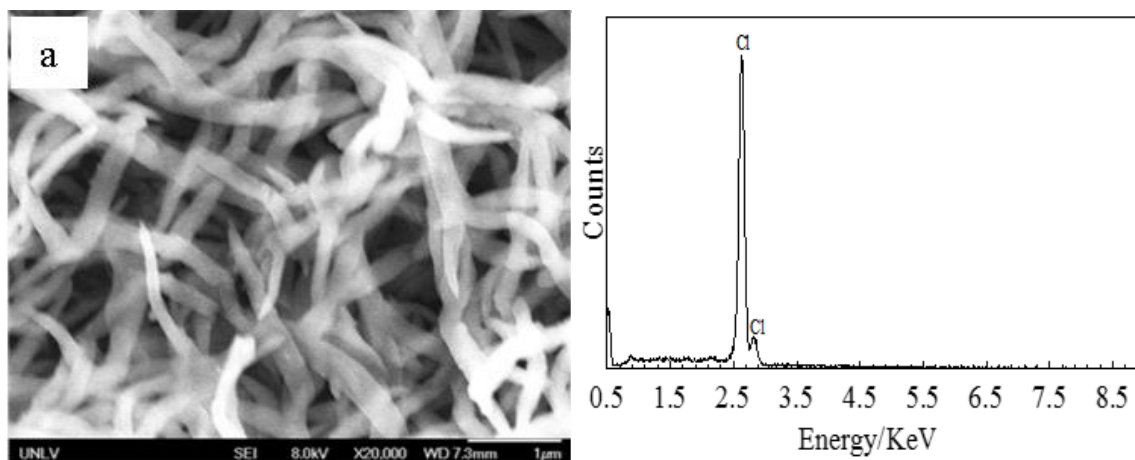


**Figure 17.** Comparison of proton dopes of (a) PANI growth, and (b) PANI/Ni after the tenth voltammetric scan in 1 M HClO<sub>4</sub>. The scan rate is 10 mV/s.

#### 3.4.4 Scanning Electron Microscopy (SEM/EDX) of PANI/Ni Composites

SEM images for the pristine polymer and PANI/Ni composites are presented in **Figure 18**. The deposition and aggregation of Ni on grafoil is not expected when deposited in PANI. Specifically, the three-dimensional structure and the ability to control the oxidation state of the polymer are utilized to disperse the Ni precursor to minimize aggregation. Previous SEM analyses of Ni deposits on compact PANI films has shown an uneven distribution of Ni consistent with the grafoil samples in **Figure 12**.<sup>24</sup> In contrast, the current voltammetric techniques utilized to grow PANI on grafoil and reduce the Ni precursor on PANI provided more control for the deposition of Ni and the formation of the PANI/Ni composite. For comparison,

the SEM image of PANI prior to Ni deposition is provided in **Figure 18a** with the SEM image of PANI/Ni composite after five deposition cycles of Ni precursor, **Figure 18b**. Both images are obtained using the same magnification, x20,000. The Ni deposits are observed on the PANI strands with some aggregation. However, the PANI/Ni composite shows a more even distribution of Ni particles along the polymer strands. The morphology of the Ni deposits contains some spherical species and longer aggregates that display sharper geometric morphologies. The Ni deposits in PANI were confirmed using EDX analyses. The data show responses from Cl for both the polymer and the PANI/Ni composite, which is consistent with trapped chloride species. The Ni deposits are visible for the PANI/Ni composite at 1.2 KeV, 7.5 KeV, and 8.3 KeV. The response from the nickel for the PANI/Ni composite is much lower than the response that was seen for the Ni deposited on grafoil. However, not all Ni deposits reside at the surface. Rather the distribution of Ni occurs throughout the three-dimensional template of the polymer.<sup>63, 74</sup> The even distribution of Ni deposits is visible with some aggregation as the Ni continues to nucleate and grow on the polymer. The data verifies that the  $\text{NiCl}_4^{2-}$  precursor was effectively reduced into PANI.



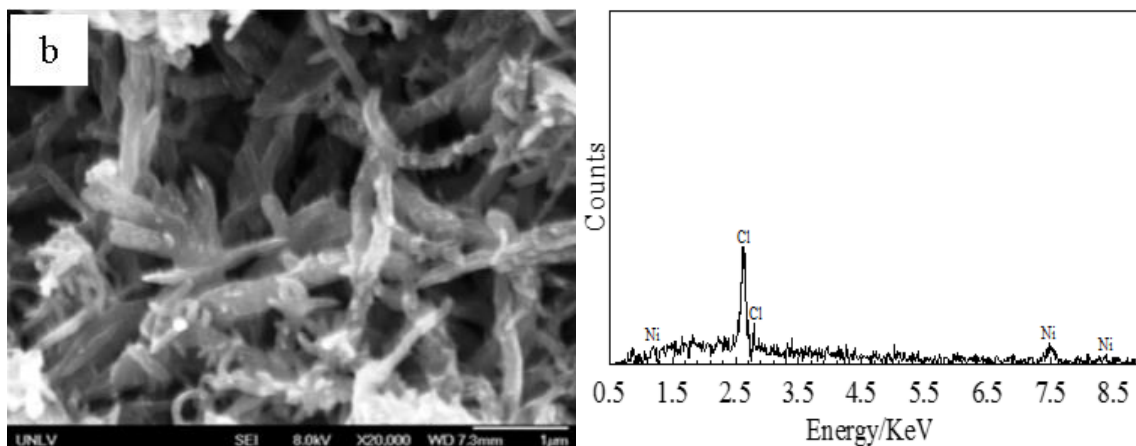


**Figure 18.** SEM image and EDX data of (a) PANI (x20,000, 8.0kV) and (b) 5 sweep step depositions of 50 mM  $\text{NiCl}_4^{2-}$  on PANI on grafoil (x20,000, 8.0kV).

### 3.4.5 PANI/Ni Electrochemistry in KOH

The PANI/Ni electrode was cycled from 0.9 V to -0.2 V for 10 voltammetric scans in 1 M KOH after each step deposition to analyze the amount of nickel deposited in the polymer. The voltammetry presented in **Figure 19** has been normalized by dividing the geometric area of each electrode into the current. For comparison to the PANI/Ni responses, the voltammetric response of the Ni disc electrode is provided in **Figure 19a**. The Ni metal disc electrode has an oxidation peak at 0.475 V and a reduction peak at 0.35 V, which is consistent with the formation the  $\text{NiOOH}/\text{Ni}(\text{OH})_2$  redox couple.<sup>73</sup> The voltammetric response of PANI on grafoil in KOH without Ni is provided in **Figure 19b**. The voltammetry demonstrates that there are no observable oxidation/reduction processes for pristine PANI. Finally, the voltammetric response for PANI/Ni electrodes after one, three, and five deposition cycles using  $\text{NiCl}_4^{2-}$  are presented in **Figures 19c-e**. The voltammetry for the PANI/Ni composite shows no discernable oxidation/reduction of Ni after the first deposition of  $\text{NiCl}_4^{2-}$ , **Figure 19c**. However, the oxidation/reduction of the Ni in PANI is resolved for the composite after three deposition cycles with redox peaks at 0.275 V and 0.375 V, **Figure 19d**. Similarly, an increase in current associated with the oxidation/reduction of

Ni in PANI is observed for the composite after the fifth deposition cycle, **Figure 19e**. The data indicates that the Ni content in PANI can be increased incrementally through the controlled reduction of the Ni precursor. Additional studies are required to determine the point at which the electrochemical reduction of the Ni precursor does not result in appreciable gains in the Ni surface area in PANI.

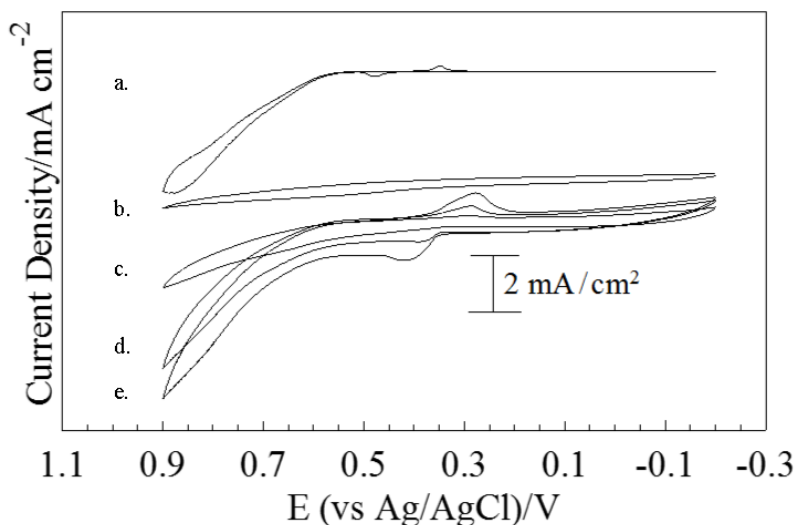
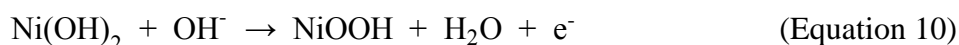
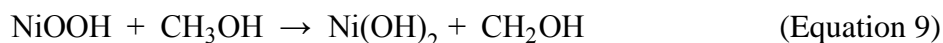


**Figure 19.** Steady-state cyclic voltammetric response of (a) Ni disc electrode (3mm), (b) response of PANI on grafoil (c) response of PANI/1 Ni, (d) response of PANI/3 Ni, and (e) response of PANI/5 Ni after the tenth voltammetric scan in solutions containing 1 M KOH; scan rate is 10mV/s.

#### 3.4.6 PANI/Ni Electrochemistry in CH<sub>3</sub>OH/KOH

The PANI/Ni electrode was cycled from 0.9 V to -0.2 V in a solution containing 1 M CH<sub>3</sub>OH and 1 M KOH, **Figure 20**. The voltammetric responses have been normalized based on the geometric area of the electrodes immersed in solution. The oxidation of methanol has been examined previously using NiO, and the following mechanism has been proposed for methanol oxidation at Ni.<sup>73, 75-76</sup>





The overall reaction for the oxidation of methanol at the PANI/Ni electrode can be represented by the following chemical equation:



The voltammetric response of a Ni disc electrode in 1 M KOH/1M CH<sub>3</sub>OH is provided for reference in **Figure 20a**. Oxidation of methanol is observed for both the cathodic and anodic scans at approximately 0.60 V. There is some hysteresis in the voltammetry indicative of differences in the potential onset and end of the oxidative processes. The Ni disc electrode has a current density of about 10 mA/cm<sup>2</sup> for the oxidation of methanol. The voltammetric scan of pristine PANI on a grafoil electrode in 1 M CH<sub>3</sub>OH/KOH is also provided in **Figure 20b**. No oxidation of methanol is observed for the forward or reverse scan without Ni. Finally, the voltammetric scans for PANI/Ni electrode after one, three, and five deposition cycles in 1 M CH<sub>3</sub>OH/KOH are provided in **Figures 20c-e**. The voltammetric response for PANI/Ni after one reduction cycle of NiCl<sub>4</sub><sup>2-</sup> shows no obvious methanol oxidation, **Figure 20c**. In contrast, after the third reduction cycle of NiCl<sub>4</sub><sup>2-</sup> into PANI, the oxidation of methanol is visible for both the forward and reverse scans at approximately 0.65 V, **Figure 20d**. Similarly, the voltammetric

response of PANI/Ni after the fifth reduction cycle of  $\text{NiCl}_4^{2-}$  into PANI follows the same pattern with increasing current density associated with increasing Ni content in PANI, **Figure 20e**. From the third reduction cycle to the fifth reduction cycle of  $\text{NiCl}_4^{2-}$  in PANI, the current density for the oxidation of methanol increases twofold, going from  $22.9 \text{ mA/cm}^2$  (third reduction cycle) to  $45 \text{ mA/cm}^2$  (fifth reduction cycle). Therefore, as more Ni is deposited in PANI, the catalytic oxidation of methanol increases. A small current response at  $0.3 \text{ V}$  is also observed after the third and fifth reduction cycles of  $\text{NiCl}_4^{2-}$ , which is consistent with the reduction of  $\text{NiOOH}$  to  $\text{Ni(OH)}_2$ .

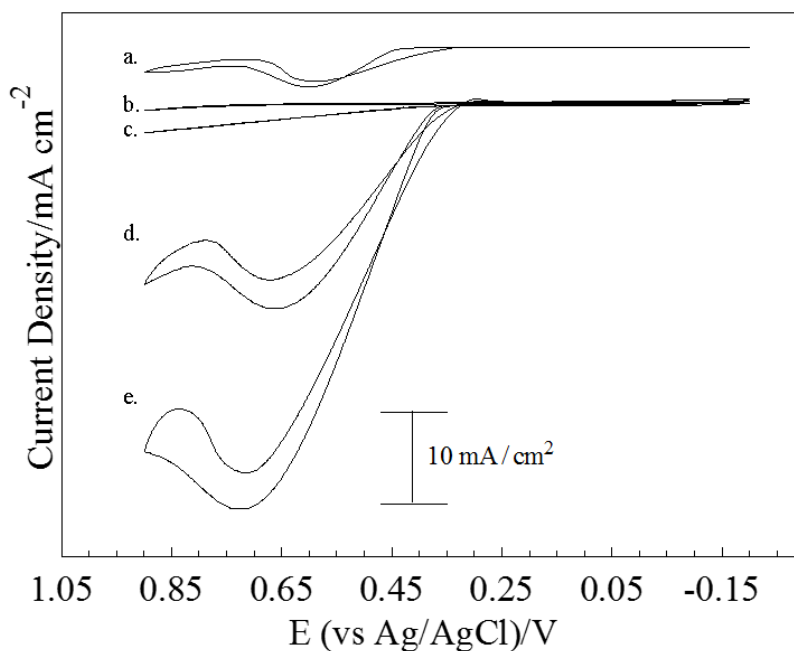


**Figure 20.** Steady-state cyclic voltammetric response of (a) response of Ni disc electrode (3mm), (b) PANI on grafoil electrode, (c) response of PANI/1 Ni, (d) response of PANI/3 Ni, and (e) response of PANI/5 Ni after the sixteen voltammetric scan in solutions containing  $1 \text{ M KOH}$  and  $1 \text{ M CH}_3\text{OH}$ ; scan rate is  $10 \text{ mV/s}$ .

The monometallic complex that forms between PANI/Ni composite shows consistent methanol oxidation in 1 M CH<sub>3</sub>OH/KOH. To analyze the long-term stability of PANI/Ni during methanol oxidation, the composite was cycled in the methanol/KOH solution for one hundred complete cycles. The methanol oxidation for the sixteenth cycle was then compared to the one hundredth cycle, **Figure 21**. From the 16<sup>th</sup> cycle to the 100<sup>th</sup> cycle, there is a decrease in current density of about 2 mA/cm<sup>2</sup>. The voltage at which the methanol oxidation occurs does not change over time, which shows the energy required for the reaction to occur remains the same. The slight decrease in current density is minimal, but may be due to slight adsorption of CO on the surface of Ni.

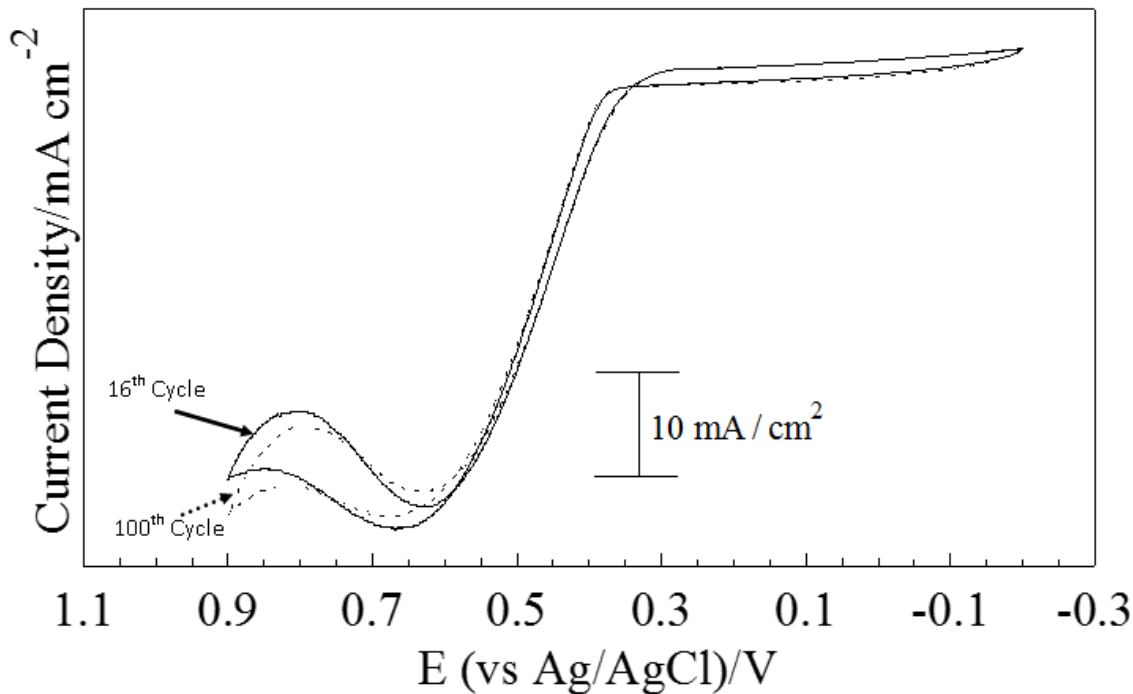


**Figure 21.** Steady-state cyclic voltammetric response of PANI/5 Ni after the sixteenth (solid line) and one-hundredth (dashed line) voltammetric scan in solutions containing 1 M KOH and 1 M CH<sub>3</sub>OH. The scan rate is 10mV/s.

### 3.4.7 PANI/NiCl<sub>2</sub> Electrochemistry in KOH versus PANI/Ni Precursor

The difference in electrochemical response between the NiCl<sub>2</sub> starting material and the Ni precursor (NiCl<sub>4</sub><sup>2-</sup>) was examined. Five deposition scans for the nickel chloride materials were deposited using two different pristine PANI coated grafoil electrodes. The electrodes were then cycled in 1 M KOH and the voltammogram is presented in **Figure 22** and the responses have been normalized using the geometric area of each electrode. PANI/NiCl<sub>2</sub> has an oxidation peak at 0.39 V and a reduction peak at 0.26 V, **Figure 22a**. The redox peaks confirm the successful deposition of NiCl<sub>2</sub> in PANI. The current density is about 0.2 mA/cm<sup>2</sup> for the redox peaks. As previously observed, PANI/Ni precursor electrode (NiCl<sub>4</sub><sup>2-</sup>) has shifted redox peaks at 0.42 V and 0.29 V, **Figure 22b**. The current density for the redox peaks is 1 mA/cm<sup>2</sup>. The current response for PANI/NiCl<sub>2</sub> is one fifth of the response of the Ni precursor in PANI in 1 M KOH. The increased current density and shifted redox peaks further indicates that the Ni precursor was formed and has an increased electrochemical response versus the NiCl<sub>2</sub> starting material.

Previous studies for the formation of PANI/Ni composites have focused on the uptake and reduction of Ni<sup>2+</sup> with limited success. Therefore, oxidation of methanol using PANI/Ni composites have been limited due to the lack of anion metal precursor needed for the controlled uptake and reduction of the metal.

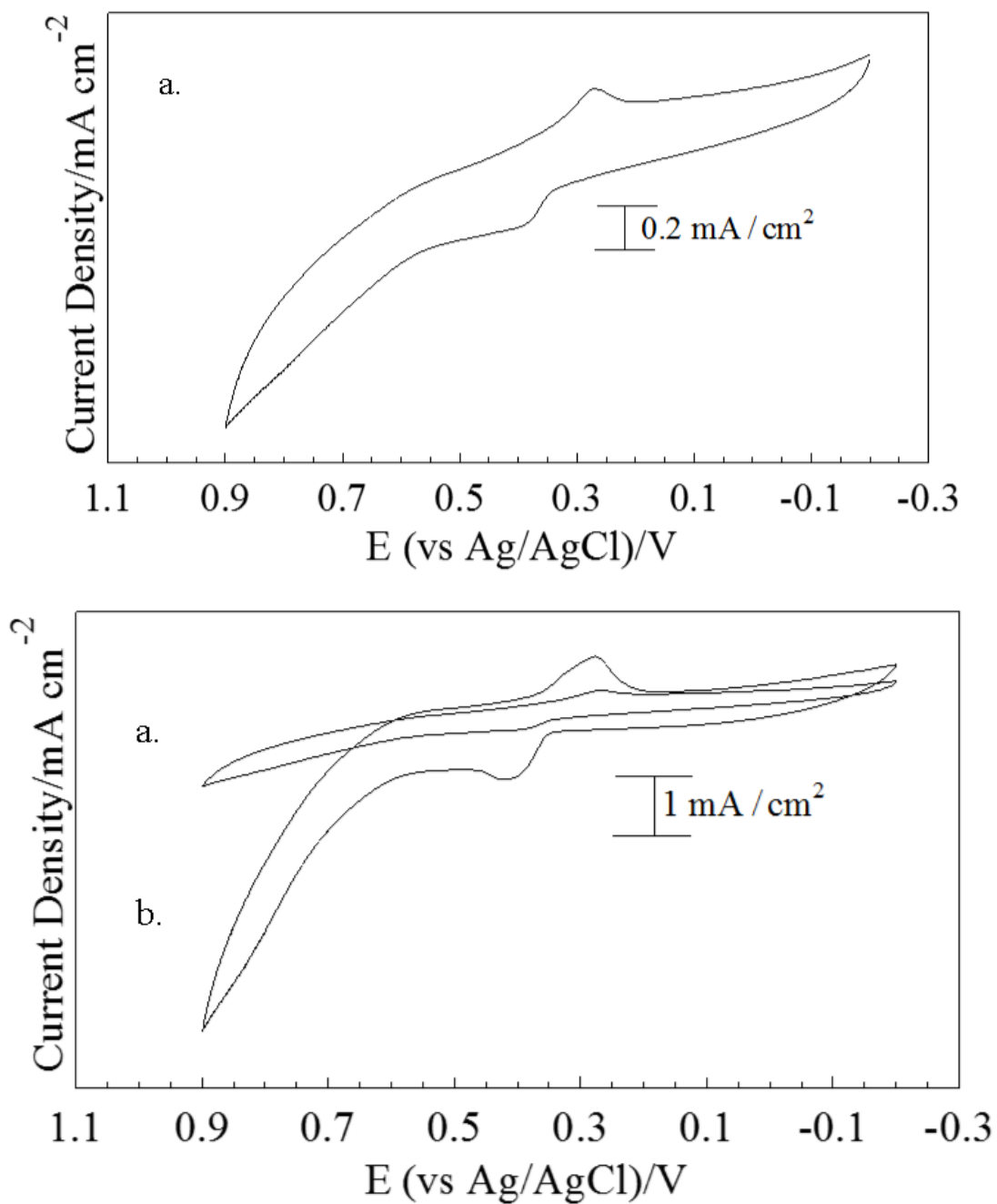


**Figure 22.** Steady-state, cyclic voltammetric response of (a) PANI/5 steps of 50 mM NiCl<sub>2</sub> and (b) response of PANI/5 steps of 50 mM NiCl<sub>4</sub><sup>2-</sup> after the tenth voltammetric scan in solutions containing 1 M KOH. The scan rate is 10mV/s.

### 3.4.8 PANI/NiCl<sub>2</sub> Electrochemistry versus PANI/NiCl<sub>4</sub> in 1 M CH<sub>3</sub>OH/KOH

The oxidation of methanol was examined for PANI/NiCl<sub>2</sub> and compared to PANI/Ni precursor to further verify the formation of the Ni precursor. The PANI/NiCl<sub>2</sub> was cycled in 1 M CH<sub>3</sub>OH/KOH from -0.2 V to 0.9 V and the resulting data was overlaid with PANI/Ni precursor, **Figure 23**. PANI/NiCl<sub>2</sub> electrode shows methanol oxidation for both the forward and reverse scans at about 0.58 V, **Figure 23a**. The oxidation response has a current density of about 1.5 mA/cm<sup>2</sup>. In contrast, PANI/Ni precursor shows methanol oxidation at approximately 0.72 V for both the forward and reverse scans, **Figure 23b**. The current density as reported earlier for PANI/Ni precursor is about 45 mA/cm<sup>2</sup> for methanol oxidation. The current density for the PANI/NiCl<sub>2</sub> is about 3% of the current density of PANI/Ni precursor for methanol oxidation, with the geometric area incorporated. Therefore, two conclusions can be made. The first conclusion is that the Ni precursor, [(CH<sub>3</sub>)<sub>2</sub>NH<sub>2</sub>]<sub>2</sub>NiCl<sub>4</sub>, is different from the starting material, which further verifies the successful synthesis of [(CH<sub>3</sub>)<sub>2</sub>NH<sub>2</sub>]<sub>2</sub>NiCl<sub>4</sub>. The second conclusion is that cation deposition of nickel, when specifically using NiCl<sub>2</sub>, shows much less catalytic activity towards methanol oxidation in comparison to the anion deposition of nickel, when specifically utilizing NiCl<sub>4</sub><sup>2-</sup>.

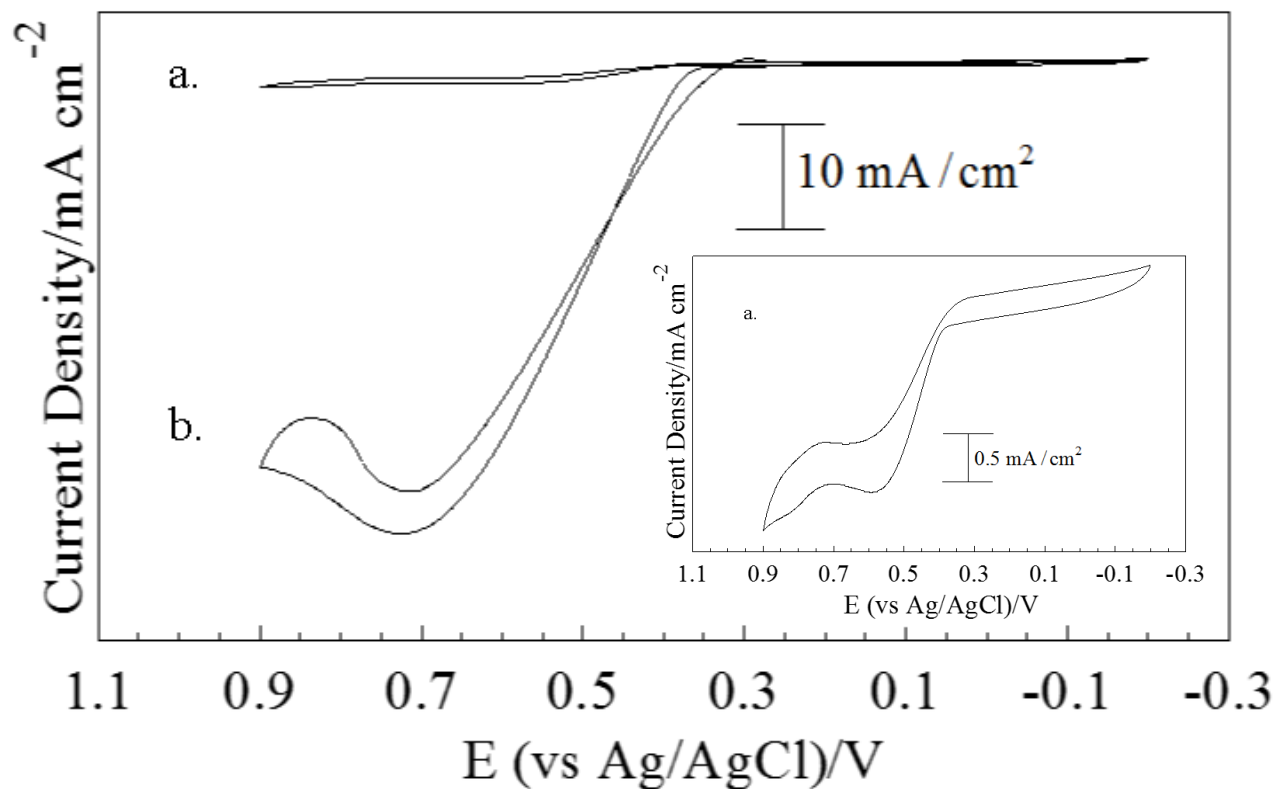


**Figure 23.** Steady-state cyclic voltammetric response of (a) PANI/5 steps of 50 mM NiCl<sub>2</sub> and (b) response of PANI/5 steps of 50 mM NiCl<sub>4</sub><sup>2-</sup> after the sixteenth voltammetric scan in solutions containing 1 M CH<sub>3</sub>OH/KOH. The scan rate is 10mV/s.

### 3.5 Conclusions

The synthesis of bis(dimethylammonium) tetrachloronickelate, [(CH<sub>3</sub>)<sub>2</sub>NH<sub>2</sub>]<sub>2</sub>·NiCl<sub>4</sub>, is demonstrated by reacting dimethylamine hydrochloride with NiCl<sub>2</sub> in the presence of chloroform. FTIR and UV/Vis analyses characterize and differentiate the starting material from the synthesized Ni precursor. The controlled electrochemical reduction of the Ni precursor is achieved and is utilized to vary Ni content on grafoil and in PANI. Proton dope analysis of Ni in PANI verifies the deposition of Ni at the nitrogen sites of the polymer. SEM images show that the morphologies of the reduced Ni precursor on grafoil and in PANI are similar. However, the PANI/Ni composite has a more even distribution of Ni particles along the polymer strands and

within the three-dimensional structure. The reduction technique utilized to deposit Ni on PANI provided a point of contact on the polymer for Ni precursor reduction so that an even distribution on the PANI strands was achieved. The oxidation/reduction of the Ni precursor on grafoil and in PANI is confirmed in 1 M KOH. A pair of redox peaks is visible between 0.2 V and 0.4 V for both Ni on grafoil and PANI/Ni composite, which is most likely due to the NiOOH/Ni(OH)<sub>2</sub> redox couple. With increasing Ni content, the current density for the redox couple increases tenfold from the first reduction scan to the fifth reduction scan of NiCl<sub>4</sub><sup>2-</sup> on grafoil and in PANI. In contrast, the current density for the redox couple of Ni on grafoil is four times larger than the current density for the redox couple of the PANI/Ni composite. This is due to the deposition of Ni on a two-dimensional surface such as grafoil versus in a three-dimensional template such as PANI. The catalytic oxidation of methanol in alkaline solution is demonstrated for both Ni deposits on grafoil and the PANI/Ni composite. The Ni disc electrode shows four times less current density for methanol oxidation in comparison to the Grafoil/Ni electrode and the PANI/Ni composite, with the geometric area incorporated. The PANI/Ni composite electrode shows a much larger current density of 45 mA/cm<sup>2</sup> than the Grafoil/Ni electrode for methanol oxidation after five reduction scans of NiCl<sub>4</sub><sup>2-</sup>. The PANI/Ni composite does not have competing secondary reactions that occur with the Grafoil/Ni electrode, which therefore allows methanol oxidation to occur more efficiently. When comparing the methanol oxidation of PANI/Ni for the starting material, NiCl<sub>2</sub>, and the synthesized Ni precursor, [(CH<sub>3</sub>)<sub>2</sub>NH<sub>2</sub>]<sub>2</sub>·NiCl<sub>4</sub>, the PANI/Ni precursor electrode shows thirty times the current density for methanol oxidation by the PANI/NiCl<sub>2</sub> electrode. The deposition of NiCl<sub>2</sub> in PANI was successful, and methanol oxidation was visible, but the cation deposition of Ni was much less successful in comparison to the anion deposition of Ni in PANI using [(CH<sub>3</sub>)<sub>2</sub>NH<sub>2</sub>]<sub>2</sub>·NiCl<sub>4</sub>. Previously published research on PANI/Ni



composites have not been as effective towards methanol oxidation because the controlled anion deposition of the polymer has not been utilized until now. Bis(dimethylammonium) tetrachloronickelate is an ideal compound for the uptake and reduction of the metal anion  $\text{NiCl}_4^{2-}$  in PANI. Using Linear Sweep Voltammetry for the deposition of this Ni precursor, the Ni content in the polymer is controlled by the oxidation/reduction of PANI. The even distribution of Ni in PANI is also accomplished using these electrochemical techniques. The Ni embedded in the polymer is then easily exploitable for controlled reactions, specifically methanol oxidation, without competing side reactions or poisoning of the metallic surface. The PANI/Ni composite is a much more economical approach for the catalytic oxidation of methanol versus the traditional PANI/noble metal composites, as nickel is less expensive and oxidizes methanol effectively.

## Chapter 4. Electrochemical Formation and Analysis of PANI/Au/Ni Composites

### 4.1 Introduction

This chapter outlines the formation and the characterization of bimetallic catalysts in PANI. Potassium tetrachloroaurate,  $K(AuCl_4)$ , and the synthesized nickel precursor bis(dimethylammonium) tetrachloronickelate,  $[(CH_3)_2NH_2]_2 \cdot NiCl_4$ , were utilized to achieve bimetallic catalysts in PANI. A 5 mM solution of  $K(AuCl_4)$  in water was freshly prepared prior to deposition. The Ni precursor was also freshly prepared prior to deposition by dissolving it in water at a concentration of 50 mM. PANI was grown on grafoil using the same parameters as mentioned in Chapter 3. Linear Sweep Voltammetry was utilized for both the simultaneous deposition of  $AuCl_4^-$  and  $NiCl_4^{2-}$  and the sequential deposition of first  $AuCl_4^-$  followed by  $NiCl_4^{2-}$ . The PANI/Au/Ni composites were then characterized by cycling the electrode in 1 M  $HClO_4$  and by SEM/EDS analyses. Finally, the oxidant and catalytic properties of the PANI/Au/Ni composites were recorded in 1 M KOH and 1 M  $CH_3OH/KOH$ , respectively using Cyclic Voltammetry.

### 4.2 Electrochemical Formation of PANI/Au/Ni Composites

#### 4.2.1 Sequential Deposition of Gold and Nickel in PANI

Sequential deposition can provide control over the amount of each metal deposited and the interaction between the metals for the formation of PANI/Au/Ni composites. For sequential deposition, the grafoil/PANI electrode was immersed in 5 mM  $K(AuCl_4)$  aqueous solution. One sweep-step deposition of 5 mM  $K(AuCl_4)$  in PANI was completed using Linear Sweep Voltammetry (LSV). The electrochemical reduction of the  $AuCl_4^-$  was initiated by holding the grafoil/PANI electrode at 1 V to oxidize the polymer. The cathodic scan began two minutes after and was terminated at -0.2 V.

Following one sweep-step deposition of 5 mM K(AuCl<sub>4</sub>), the PANI/Au electrode was immersed in 50 mM [(CH<sub>3</sub>)<sub>2</sub>NH<sub>2</sub>]<sub>2</sub>·NiCl<sub>4</sub> aqueous solution, and the same LSV technique was again utilized to deposit five consecutive steps of [(CH<sub>3</sub>)<sub>2</sub>NH<sub>2</sub>]<sub>2</sub>·NiCl<sub>4</sub>. Between each sweep-step deposition, the working electrode along with the reference and counter electrodes were thoroughly rinsed with water. The voltammetric responses were overlaid for comparison, **Figure 24**. The dotted line in the figure represents the first and only reduction scan of the gold in PANI, where two cathodic peaks are visible at 0.15 V and -0.3 V. These are consistent with the desorption of OH<sup>-</sup> ions and the reduction of AuO.<sup>77</sup> This reduction process of Au can be explained by the following equations.<sup>77</sup>



The solid line in the figure represents the first of five reduction scans of Ni on Au. The cathodic response resembles previous voltammograms obtained from depositing Ni in PANI from Chapter 3 using the same parameters. Two cathodic peaks are resolved at 0.50 V and about 0.075 V. These reduction peaks are slightly shifted in comparison to the voltammetric responses observed from the direct reduction of Ni in PANI without gold. This slight voltammetric shift implies that Ni is depositing on Au that is embedded in PANI rather than at the nitrogen sites of the polymer. The current response for Au reduction in PANI is about four times that of Ni, which further confirms the favorable reduction of Au in PANI.

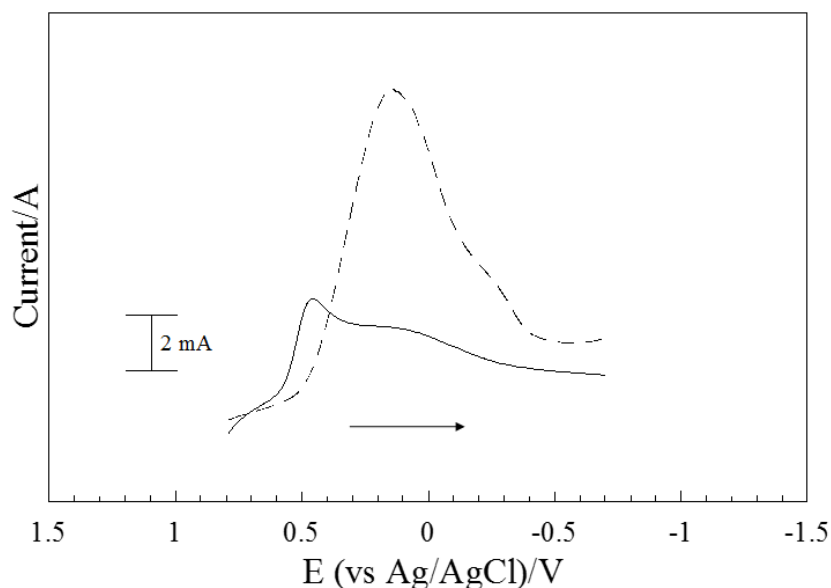


**Figure 24.** LSV voltammetric response of the 1<sup>st</sup> and only step scan of 5 mM AuCl<sub>4</sub> deposited on PANI on Grafoil (dotted line) and of the 1<sup>st</sup> of five step scans of 50 mM NiCl<sub>4</sub> deposited on PANI/Au (solid line). The scan rate is 10 mV/s.

#### 4.2.2 Proton Dope Analysis of PANI/Au/Ni Composite

Following PANI growth on grafoil and after each metal deposition, a proton dope was run on the electrode to verify the deposition of metal particles at the nitrogen sites of the polymer. To perform the proton dope, the electrode was cycled for ten full cycles in 1 M HClO<sub>4</sub>. The cyclic voltammograms of each proton dope were overlaid for comparison, **Figure 25**. The proton dope following PANI growth is given in **Figure 25a**. The oxidation/reduction peaks for the proton expulsion and uptake occur at 0.15 V and 0.05 V, respectively. The anion expulsion and uptake occur at 0.76 V and 0.71 V, respectively. Following the reduction of Au, the oxidation/reduction processes for the proton and anion expulsion/uptake decreased in current, but there was no shift in potential in comparison to the proton dope following PANI growth on the electrode, **Figure 25b**. After five reduction steps of Ni, the redox pair for the proton expulsion and uptake shift to more positive potentials, **Figure 25c**. The shift to more positive potentials

indicates that less energy is required for the uptake and expulsion of protons at the nitrogen sites of the polymer with the addition of Ni. For the uptake and expulsion of anions, there is a shift to more negative potentials for the redox processes. Therefore, following Ni deposition, more energy is required for the uptake and expulsion of anions at the nitrogen sites of the polymer. The decrease in current for the proton/anion uptake and expulsion indicates that there are less nitrogen sites available in the polymer following Ni reduction. Therefore, both Au and Ni deposit at the nitrogen sites of the polymer according to the proton dope analysis. SEM imaging and EDX analyses of the PANI/Au/Ni films are necessary to verify the sequential deposition of Au and Ni in PANI as well as to verify the reduction sites of each metal in PANI.

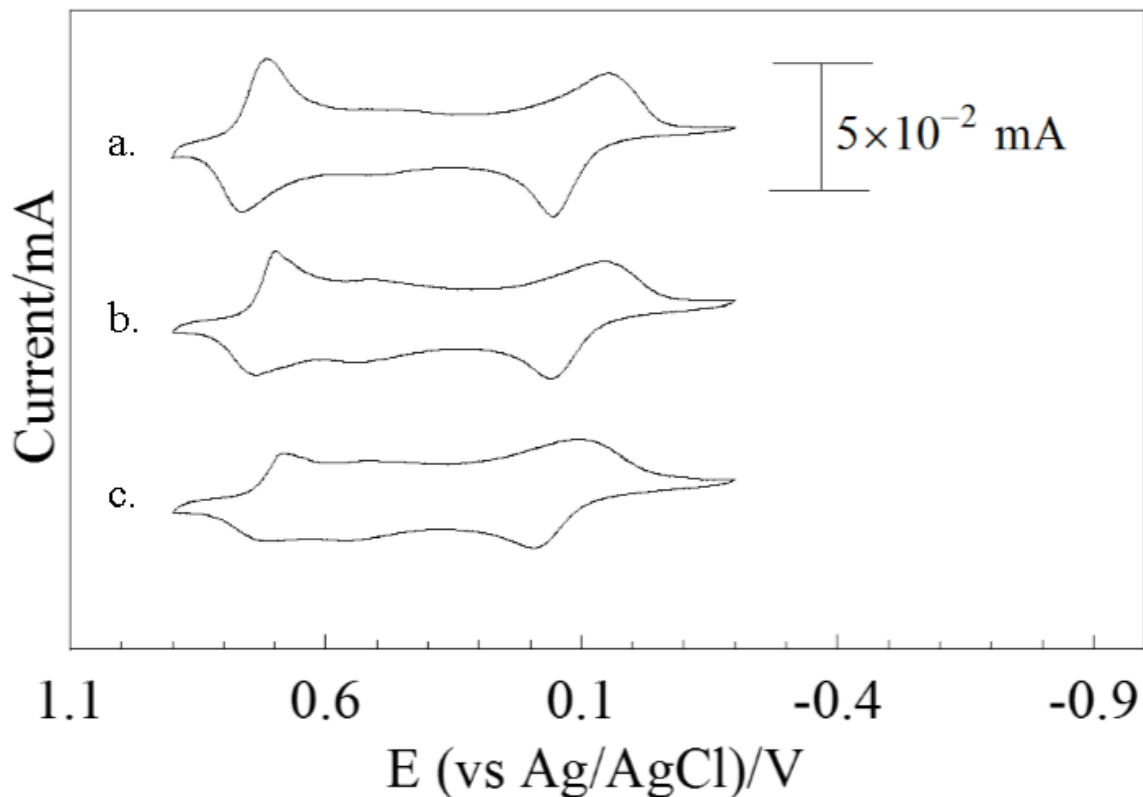


**Figure 25.** Comparison of proton dopes of (a) PANI growth, (b) PANI/1 Au, and (c) PANI/1Au/5Ni after the tenth voltammetric scan in 1 M HClO<sub>4</sub>. The scan rate is 10 mV/s.

### 4.3 Scanning Electron Microscopy (SEM/EDX) of PANI/Au/Ni Composites

SEM/EDX analyses were utilized to further characterize the PANI/Au/Ni composites and to understand the interaction of the metallic deposits with each other and the polymer. SEM images and the EDX data for PANI/Au/Ni composites are presented in **Figure 26**. All images are presented at the same magnification of x6000 with an accelerating voltage of 8 kV. The SEM image and EDX data for pristine PANI are shown in **Figure 26a** for comparison. After one sweep-step deposition of Au in PANI, the Au particles are visibly embedded in the polymer, **Figure 26b**. The Au particles are about 0.5  $\mu\text{m}$  in size and are spread along the polymer strands, with some aggregation. EDX analysis confirms the presence of Au in PANI. The Au deposits were identified at 1.7 KeV, 2.2 KeV, 2.3 KeV, and 9.9 KeV. After five sweep-step depositions of Ni in the PANI/Au composite, Ni particles are seen evenly dispersed on the gold and along the polymer strands, **Figure 26c**. The sizes of the particles are much smaller than the gold particles at about 0.1  $\mu\text{m}$  or less. The Ni deposits have mostly sharp geometric morphologies on the gold deposits and on the polymer strands. The presence of nickel on the gold was confirmed using EDX analyses. The nickel deposits for the PANI/Au/Ni composites were identified at 0.82 KeV, 7.5 KeV, and 8.3 KeV. This is consistent with the studies done on Ni precursor on grafoil and PANI/Ni precursor composite. The EDX data show a strong response from gold following the five sweep-step depositions of nickel precursor, indicating the Ni particles do not fully encapsulate the Au particles, but rather form a bimetallic species. Previous SEM/EDX studies on Au—Ni bimetallic catalysts have shown similar results, where the Ni particles attached to the surface of the Au particles in an alloyed formation.<sup>78-79</sup> These previous studies also touched on the fact that even at higher concentrations of Ni, Au particles still have high surface composition for these bimetallic species.

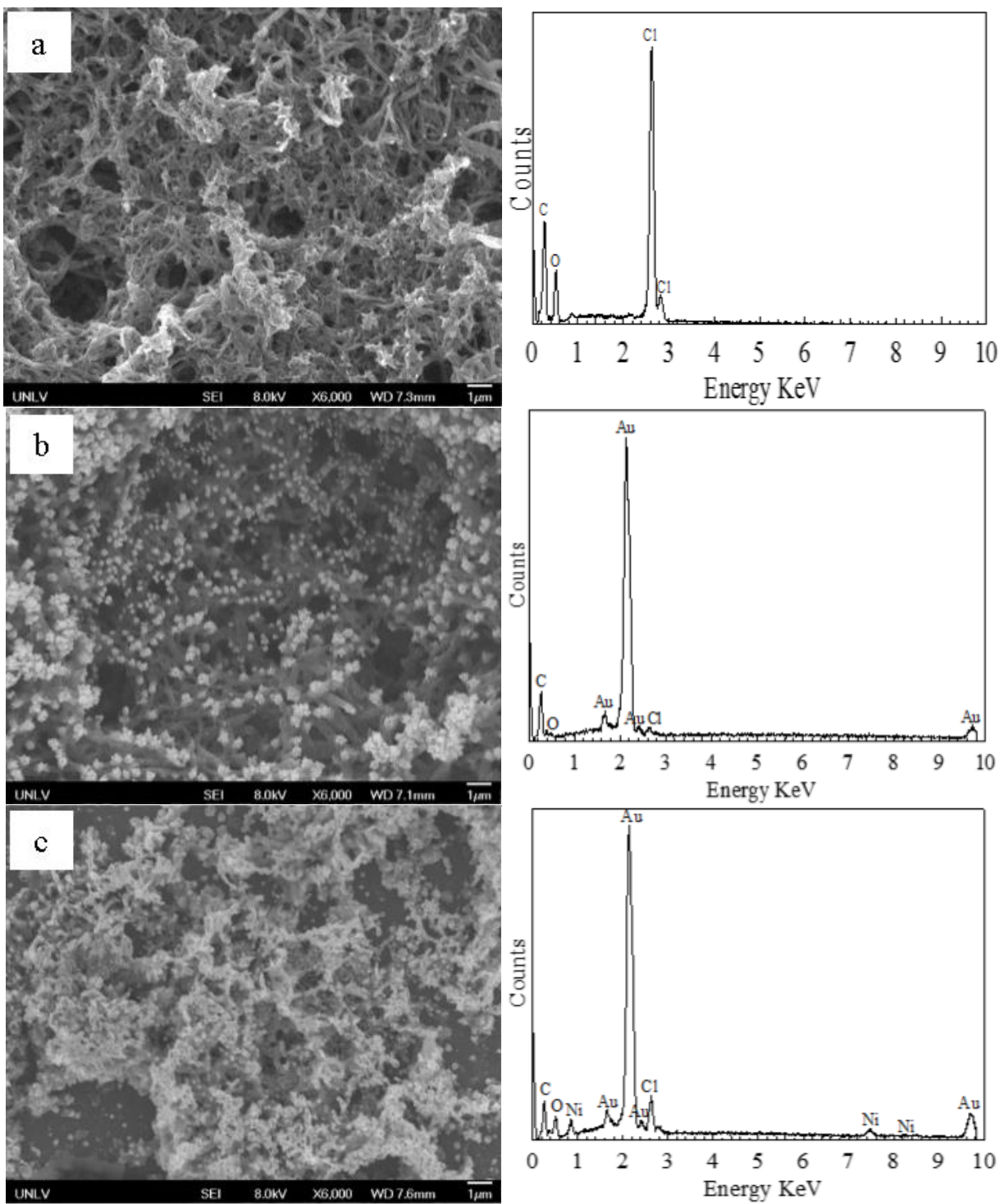


**Figure 26.** SEM image and EDX analyses of (a) pristine PANI ( $\times 6000$ ), (b) PANI/1 Au composite ( $\times 6000$ ), and (c) PANI/1Au/5 Ni composite ( $\times 6000$ ).

At larger magnifications, the Au—Ni bimetallic species in PANI show round Au with Ni deposits with more defined angular morphologies attached to the Au surface, **Figure 27**. The Au particles are attached to the strands of the polymer. This figure better defines the bimetallic morphology of the PANI/Au/Ni composite. Further electrochemical characterization in basic solutions are necessary to determine the characteristics of the Ni and Au deposits in the PANI/Au/Ni composites.

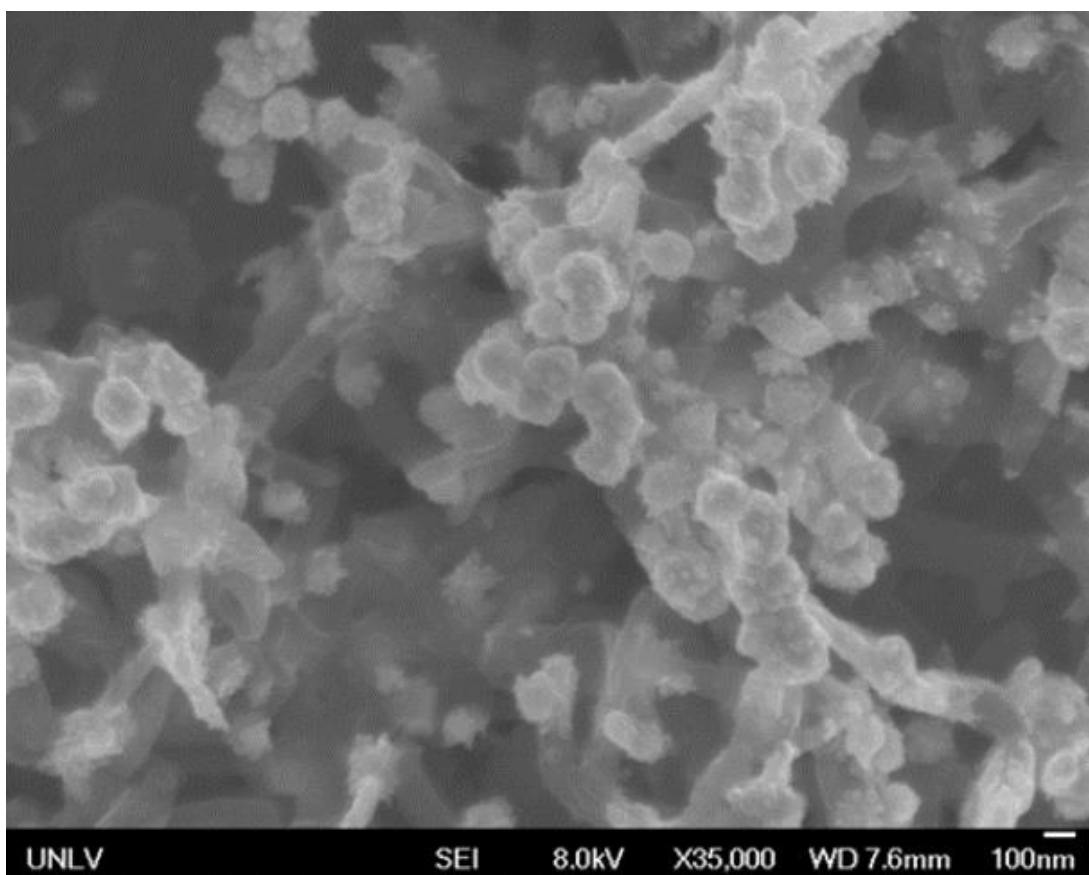


**Figure 27.** SEM image of PANI/Au/Ni composites at a magnification of x35,000.



## 4.4 Electrochemical Analysis of PANI/Au/Ni Composites

### 4.4.1 PANI/Au/Ni Electrochemical Analysis in KOH

Following the growth of the polymer and each sequential deposition of first one sweep step of 5 mM AuCl<sub>4</sub><sup>-</sup> and then five sweep steps of 50 mM NiCl<sub>4</sub><sup>2-</sup>, the PANI composite was electrochemically cycled in 1 M KOH (pH 14.0). The responses were compared for the deposition of gold and then nickel in 1 M KOH with respect to the area of the electrode, **Figure 28**. The cyclic voltammetric responses for an Au disc electrode and a Ni disc electrode in 1 M KOH are shown in **Figure 28a** and **g** for comparison. Two reduction peaks for the Au disc electrode cathodic scan appear at 0.095 V and -0.185 V, with current densities of 2.94E-02 mA/cm<sup>2</sup> and 3.09E-02 mA/cm<sup>2</sup>, respectively. There are two oxidation peaks for the anodic scan of the Au disc electrode at 0.4 V and -0.105 V, with current densities at 2.02E-2 mA/cm<sup>2</sup> and 5.06E-3 mA/cm<sup>2</sup>, respectively. The current density is much smaller than all other electrode responses in KOH for the Au disc electrode, therefore, the response in comparison appears as a straight line, **Figure 28a**. The redox couples observed for the Au disc electrode have been previously associated with the following chemical reaction.<sup>80</sup> The redox couples are associated with the adsorption of OH<sup>-</sup> on the surface of the gold.



The cyclic voltammetric response of the Ni disc electrode in 1 M KOH for **Figure 28g** shows the same redox peaks reported in **Figure 13a** from **Chapter 3**, where the reduction and oxidation peaks are observed at 0.35 V and 0.50 V, respectively. The cyclic voltammetric response of PANI on the grafoil electrode in 1 M KOH prior to metal deposition is given in

**Figure 28b.** There are no visible oxidation/reduction peaks for PANI on grafoil in the potential range of -0.2 V to 0.9 V. Following one sweep step deposition of 5 mM  $\text{AuCl}_4^-$ , the cyclic voltammetric response of PANI/Au composite in 1 M KOH is provided in **Figure 28c**. A very small reduction peak is visible at 0.076 V and a small oxidation peak is at -0.112 V. The shifted peaks are consistent with the deposition of metal in PANI. No other redox peaks are visible for the PANI/Au composite. The three-dimensional structure of the polymer allows for the gold to evenly disperse inside the layers of the polymer, which causes the current density response in 1 M KOH to be much less in comparison to the Au disc electrode.

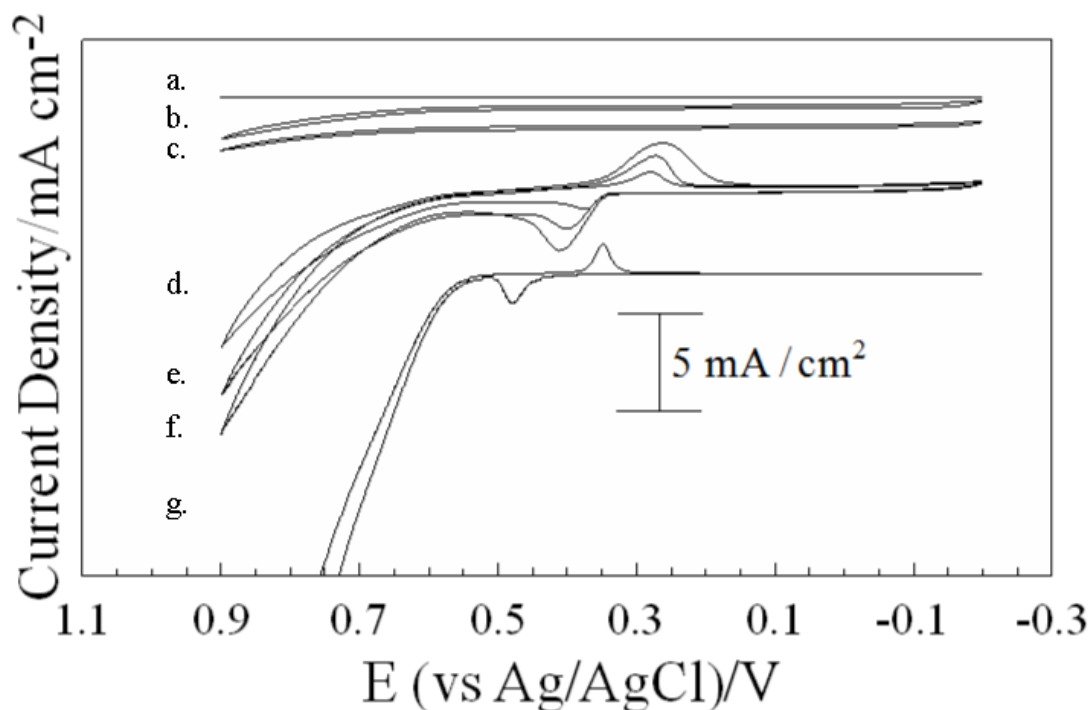


**Figure 28.** Steady-state cyclic voltammetric response of (a) a planar Au disc electrode ( $d=3\text{mm}$ ), (b) PANI on grafoil, (c) PANI/1Au composite, (d) PANI/1Au/1Ni composite, (e) PANI/1Au/3Ni composite, (f) PANI/1Au/5Ni composite, (g) a planar Ni disc electrode ( $d=3\text{mm}$ ) after the tenth voltammetric scan in solution containing 1 M KOH. The scan rate is 10mV/s.

Finally, the cyclic voltammetric responses for PANI/Au composite following the first, third, and fifth reduction of Ni precursor in 1 M KOH are provided in **Figure 28d-f**. The first deposition of Ni in PANI/Au reveals a reduction peak at 0.256 V and the corresponding oxidation peak for the anodic scan at 0.408 V. The current density for the first deposition is 0.75 mA/cm<sup>2</sup> for the reduction peak and 0.88 mA/cm<sup>2</sup> for the oxidation peak. After three and five sweep step depositions of Ni on PANI/Au, the redox peaks occur at the same voltage. However, the current density increases 3-fold from the first deposition to the fifth deposition. The increase in current density in KOH coincides with increased Ni deposits on the PANI/Au composite. The data shows that the Ni content in PANI/Au can be increased incrementally through the controlled reduction of the Ni precursor. Further analysis is required to determine the appropriate amount of Ni to deposit in the PANI/Au composite that is necessary for the catalytic oxidation of methanol.

#### 4.4.2 PANI/Au/Ni Electrochemical Analysis in 1 M CH<sub>3</sub>OH/KOH

The PANI/Au/Ni composite was analyzed for methanol oxidation by cycling the electrode from 0.9 V to -0.2 V in a solution containing 1 M CH<sub>3</sub>OH/KOH, **Figure 29**. The responses of the electrodes have been normalized based on their geometric area. For comparison, an Au disc electrode and a Ni disc electrode were run in the same solution using the same parameters and the cyclic voltammograms are provided in **Figure 29a** and **d**. No oxidation of methanol is visible for the Au disc electrode in these parameters, **Figure 29a**. The Ni disc electrode shows methanol oxidation at about 0.6 V with a current density of about 10 mA/cm<sup>2</sup>, **Figure 29d**. PANI grown on grafoil showed no voltammetric response for methanol oxidation, **Figure 29b**. Following one sweep step deposition of 5 mM Au, the cyclic voltammetric response in 1 M CH<sub>3</sub>OH/KOH also showed no response for the oxidation of methanol, **Figure 29c**. Finally, the cyclic voltammetric scans for PANI/Au/Ni composite following one, three, and five

deposition cycles of 50 mM  $\text{NiCl}_4^{2-}$  in 1 M  $\text{CH}_3\text{OH/KOH}$  are provided in **Figure 29e-g**. For one reduction cycle of  $\text{NiCl}_4^{2-}$ , methanol oxidation occurs at 0.7 V with a current density of about 15  $\text{mA/cm}^2$ , which can be seen in **Figure 29e**. The third and fifth reduction cycle of  $\text{NiCl}_4^{2-}$  into PANI/Au composite shows methanol oxidation at 0.79 V with current densities of about 30  $\text{mA/cm}^2$  for the third reduction cycle and about 33  $\text{mA/cm}^2$  for the fifth reduction cycle, **Figure 29f and g**. The third reduction cycle to the fifth reduction cycle of  $\text{NiCl}_4^{2-}$  does not have much change in methanol oxidation. Since there are only a finite amount of Au deposits and much less nitrogen sites on the polymer available for metal deposition, only so much nickel can deposit on the PANI/Au composite. In contrast, when Ni is deposited directly on PANI without Au, the three-dimensional polymer film has several nitrogen sites open for the Ni to interact with even after five deposition cycles. Therefore, the  $\text{NiCl}_4^{2-}$  reduces on Au and on any available nitrogen sites of the polymer that Au did not physically block following reduction of this metal.

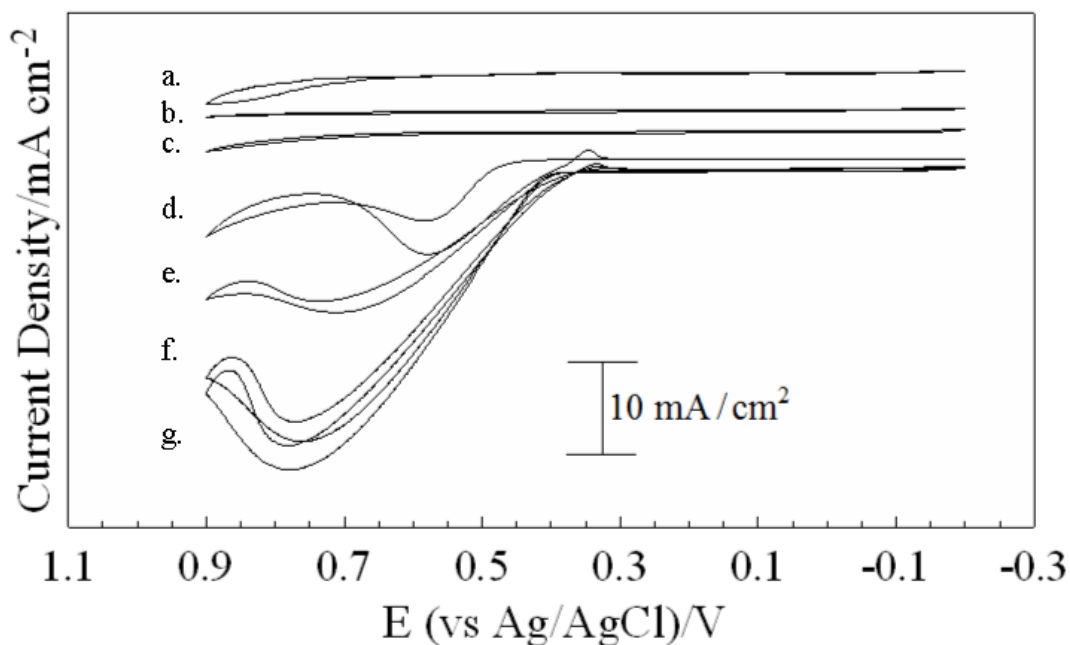


**Figure 29.** Steady-state cyclic voltammetric response of (a) a planar Au disc electrode, (b) PANI on grafoil, (c) PANI/1Au composite, (d) a planar Ni disc electrode, (e) PANI/1Au/1Ni composite, (f) PANI/1Au/3Ni composite, (g) PANI/1Au/5Ni composite after the sixteenth voltammetric scan in solution containing 1 M CH<sub>3</sub>OH/KOH. The scan rate is 10mV/s.

#### 4.5 Comparison of Catalytic Activity of PANI/Metallic Composites

##### 4.5.1 Stability of Bimetallic Catalysts

The bimetallic complex that forms between Au and Ni on the PANI/Au/Ni composite allows for consistent methanol oxidation in 1 M CH<sub>3</sub>OH/KOH. Au does not normally show catalytic activity towards methanol oxidation. Ni on the surface of gold allows for the adsorbed oxygen to leave the surface of the metal as CO<sub>2</sub> and reduce the poisoning of the surface with adsorbed CO.<sup>78</sup> To analyze the stability of the PANI/Au/Ni composites, the composite electrode was placed in 1 M CH<sub>3</sub>OH/KOH and electrochemically cycled for one hundred segments. The results are reported in **Figure 30**. A Ni disc electrode was plotted for comparison, **Figure 30a**. The cyclic voltammetric response of the PANI/Au/Ni composite after the 100<sup>th</sup> cycle (dotted line) shows consistency with the current density for the oxidation of methanol in comparison to

the 16<sup>th</sup> cycle (solid line), **Figure 30b**. Only a very slight positive shift in potential of about 0.035 V occurs at the point of methanol oxidation by the 100<sup>th</sup> cycle. This positive shift shows that after several cycles in methanol, less energy is required for the oxidation of methanol to occur. This stability in the PANI/bimetallic composite for methanol oxidation proves the Au—Ni complex works together to reduce poisoning during methanol oxidation.

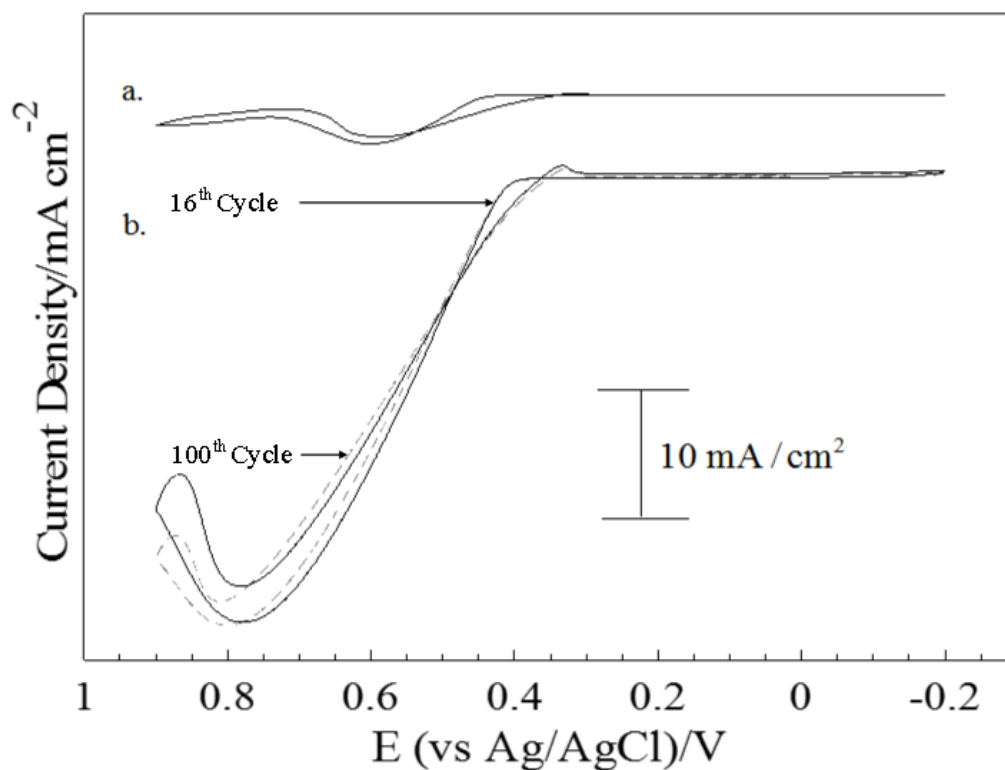


**Figure 30.** Steady-state cyclic voltammetric response of (a) Ni disc electrode ( $d=3\text{mm}$ ) and (b) response of PANI/1 Au/5 Ni after the sixteenth (solid line) and one-hundredth (dashed line) voltammetric scan in solutions containing 1 M KOH and 1 M  $\text{CH}_3\text{OH}$ . The scan rate is  $10\text{mV/s}$ .

#### 4.5.2 Comparison of Methanol Oxidation for All Composites

PANI/Au/Ni composites showed good catalytic activity and great stability towards the oxidation of methanol. In contrast, PANI/Ni composites were much more effective towards methanol oxidation, but less stable over long periods of time. **Figure 31** shows a comparison of the current densities of Ni on grafoil, PANI/Ni, and PANI/Au/Ni composites in methanol. A Ni disc electrode was added to the figure to compare the responses, **Figure 31a**. For all other electrodes with the Ni precursor deposited, the voltage where methanol oxidation occurs is shifted more positive in comparison to the nickel disc electrode. Grafoil/Ni shows very small, and mostly unresolved methanol oxidation, **Figure 31b**. PANI/Ni shows the largest current density and most resolved response for methanol oxidation, **Figure 31d**. PANI/Au/Ni composite

sits in between the Grafoil/Ni and PANI/Ni, with the second largest current density for methanol oxidation, **Figure 31c**. The PANI/Au/Ni composite shows methanol oxidation shifted to the most positive potential in comparison to the Grafoil/Ni and PANI/Ni electrodes. PANI/Ni proves to be the most efficient electrode for the catalytic electrooxidation of methanol. However, with the addition of Au and formation of the Au—Ni bimetallic species in PANI, the catalytic stability over longer periods of time for the PANI/Au/Ni composite during methanol oxidation is slightly greater than PANI/Ni. Finally, the higher current density for PANI/Ni when compared to PANI/Au/Ni suggests that the inclusion of Au reduces the overall catalytic efficiency in comparison to Ni alone.

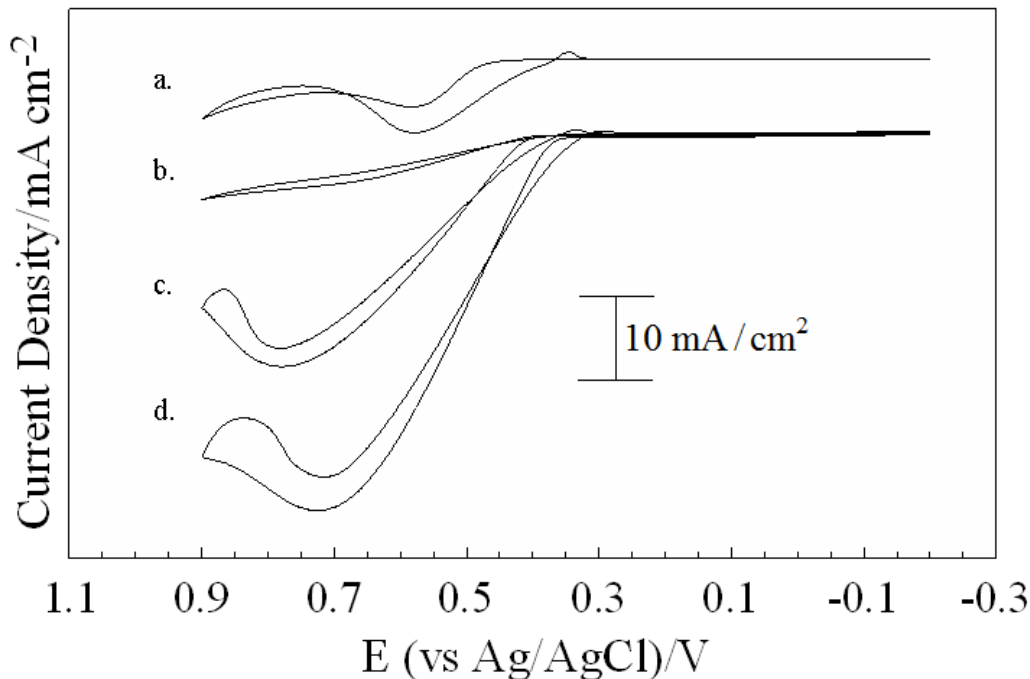


**Figure 31.** Steady-state cyclic voltammetric response of (a) a planar Ni disc electrode (b) Grafoil/5Ni electrode (c) Grafoil/PANI/1Au/5Ni composite, and (d) Grafoil/PANI/5Ni composite after the sixteenth voltammetric scan in solution containing 1 M CH<sub>3</sub>OH/KOH. The scan rate is 10mV/s.



## 4.6 Conclusions

The controlled electrochemical reduction of Au and Ni in PANI to form the PANI/Au/Ni bimetallic composite is achieved. Proton dope analysis shows Ni reduces at Au as well as at the open nitrogen sites of the polymer. The initial deposition of Au in the polymer largely blocks nitrogen sites in the polymer, which reduces sites that would be available for reaction with the Ni deposits. This is seen in the decrease in current for the proton dope analysis following Au reduction. However, nitrogen sites free from Au deposits in the polymer can still be oxidized and reduced. Therefore, the Ni deposits on Au particles as well as existing nitrogen sites of the polymer, which is verified by the decrease in current and shift in potential at the nitrogen sites for the PANI/Au/Ni composite proton dope analysis. SEM images confirm interaction between Au and Ni and the polymer. The Au particles are evenly distributed in the polymer with small Ni particles on the surface. The images verify that Ni deposition occurs on Au and at open nitrogen sites in the polymer. The deposition of both Au and Ni is confirmed using the normal oxidation/reduction of the Au and Ni in 1 M KOH. A redox pair for the PANI/Au composite is visible at 0.076 V and -0.112 V, which is consistent with the adsorption of OH<sup>-</sup> on gold. A redox pair is observed at 0.256 V and 0.408 V following the deposition of Ni into PANI/Au. The shift in potential is consistent with Ni deposition on Au particles and the NiOOH/Ni(OH)<sub>2</sub> redox couple. With increasing Ni depositions, the current density for the redox couple increases 3-fold from the first deposition to the fifth deposition on the PANI/Au composite. The first reduction step of Ni is more visible when deposited on PANI/Au composite rather than just PANI due to the overall increased surface area that occurs with the formation of the Au—Ni bimetallic complex in PANI. The catalytic oxidation of methanol in alkaline solution is also achieved for the PANI/Au/Ni composite. Methanol oxidation for the PANI/Au/Ni composite occurs at 0.79 V

with current a current density of about 33 mA/cm<sup>2</sup> by the fifth reduction cycle of the Ni precursor. There is little change in current density from the third to the fifth reduction cycle of the Ni precursor in the PANI/Au composite. The data suggests that Ni deposition is limited by the available Au surface area and nitrogen sites in the PANI/Au composite. Therefore, the current density for methanol oxidation reaches a constant by the fifth deposition of Ni. The stability of the PANI/Au/Ni composite is demonstrated after cycling the electrode for 100 segments in 1 M CH<sub>3</sub>OH/KOH. The current density does not change appreciably for methanol oxidation for PANI/Au/Ni. The stability of the PANI/bimetallic suggests that surface poisoning is minimized relative to the PANI/Au composites for methanol oxidation. In contrast, the current density for the catalytic oxidation of methanol for the PANI/Ni composite does decrease very slightly after cycling for 100 segments in 1 M CH<sub>3</sub>OH/KOH. However, the current density with respect to surface area for the catalytic oxidation of methanol is larger than the PANI/Au/Ni composite, which shows that the PANI/Ni composite is more active towards the catalytic oxidation of methanol in comparison to the PANI/Au/Ni composite.

## Chapter 5. Summary and Conclusions

The successful synthesis of bis(dimethylammonium) tetrachloronickelate,  $[(\text{CH}_3)_2\text{NH}_2]_2 \cdot \text{NiCl}_4$ , was demonstrated and confirmed by FTIR and UV/Vis analyses. The controlled electrochemical reduction of the Ni precursor was achieved and was utilized to vary Ni content on grafoil, in PANI, and in PANI/Au composites. Proton dope analysis of Ni in PANI and Ni in PANI/Au was conducted to determine the change in the redox processes at the nitrogen sites of the polymer associated with Ni deposition. Ni and Au metal reduction in PANI showed a decrease in proton doping for both PANI/Ni and PANI/Au/Ni composites, which indicates successful deposition of metallic species at the nitrogen sites of the polymer. SEM images showed the morphologies of the reduced Ni precursor are similar no matter the site of deposition. However, PANI allowed for the even distribution of metallic species versus a grafoil electrode. The SEM images of the PANI/Ni composite showed an even distribution of Ni particles along the polymer strands and within the three-dimensional structure. The SEM images of the PANI/Au/Ni composite showed Ni deposits surrounding the Au particles forming an Au—Ni bimetallic complex. Ni deposits were also visible along the polymer strands where the amine nitrogen groups were available for oxidation and reduction processes. The reduction technique utilized to deposit Au and Ni on PANI provided a point of contact on the polymer for metal precursor reduction so that an even distribution on the PANI strands was achieved. By utilizing the normal oxidation/reduction of Au and Ni in 1 M KOH, the deposition of both metallic species was confirmed. Redox pairs were visible for PANI/Ni and PANI/Au/Ni composites in KOH, which confirm the deposition in PANI. Increasing Ni depositions for both composites were accompanied by increased current densities for the  $\text{NiOOH}/\text{Ni}(\text{OH})_2$  redox couple. In contrast to PANI/Ni composites, Ni deposition on PANI/Au composites showed larger current

densities for the redox couple in KOH due to the overall increased surface area with the formation of Au—Ni bimetallic complexes in PANI. All composites showed methanol oxidation with high current densities and little to no surface poisoning. Grafoil/Ni electrode showed methanol oxidation with competing water oxidation processes. The PANI/Ni and PANI/Au/Ni composites did not have competing secondary reactions that occurred with the Grafoil/Ni electrode, which therefore allowed methanol oxidation to occur more efficiently. PANI/Ni composites showed the largest current density for methanol oxidation in comparison to all electrodes and composites. Prior to Ni deposition for the PANI/Au composite, no catalytic activity occurred in methanol. With the addition of Ni, bimetallic Au—Ni complex allowed for the successful oxidation of methanol with little to no surface poisoning. The PANI/Au/Ni composite showed methanol oxidation at more positive potentials in comparison to Grafoil/Ni and PANI/Ni electrodes. Therefore, PANI/Au/Ni composites required the least amount of energy for the oxidation of methanol to occur in alkaline solutions. Future research of these PANI/metallic and PANI/bimetallic composites may include uses for direct methanol fuel cells (DMFCs) due to their stability during the catalytic oxidation of methanol. Overall, the utilization of the synthesized Ni precursors for the anion doping of PANI was successful. PANI enhanced the catalytic efficiency of the  $\text{NiCl}_4^{2-}$  precursors by shielding the metallic species from competing secondary reactions in methanol. With the reduction of  $\text{AuCl}_4^-$  metal precursors to form PANI/Au—Ni bimetallic composites, the methanol oxidation reaction occurred at more positive potentials, indicating the bimetallic complex works as a decent catalyst for the oxidation of methanol.

The hypothesis for this research was directed towards proving the controlled deposition of metallic species, specifically Ni and Au—Ni bimetallic complexes, in PANI would produce

composites with enhanced catalytic activity in methanol. Previous research on PANI/Ni and PANI/Au composites have not been as effective towards the oxidation of methanol in alkaline solution because the controlled anion deposition of the polymer has not been utilized until now. By using the anion doping of the polymer and the LSV reduction technique, PANI/Ni and PANI/Au/Ni composites were achieved and showed enhanced catalytic activity for methanol oxidation in comparison to Ni on grafoil and PANI/Au composites. Both PANI/Ni and PANI/Au/Ni composites may be utilized for future research in direct methanol fuel cells based on their effectiveness toward the catalytic oxidation of methanol.

## References

1. Hatchett, D. W.; Josowicz, M.; Janata, J., Electrochemical Formation of Au Clusters in Polyaniline. *Chem. Mater.* **1999**, *11*, 2989-2994.
2. Hatchett, D. W.; Millick, N. M.; Kinyanjui, J. M.; Pookpanratana, S.; Bar, M.; Hofmann, T.; Luinetti, A.; Heske, C., The electrochemical reduction of PdCl<sub>4</sub><sup>2-</sup> and PdCl<sub>6</sub><sup>2-</sup> in polyaniline: Influence of Pd deposit morphology on methanol oxidation in alkaline solution. *Electrochimica Acta* **2011**, *56* (17), 6060-6070.
3. Schwartz, I. T.; Jonke, A. P.; Josowicz, M.; Janata, J., Polyaniline Electrodes with Atomic AuPd<sub>1</sub> Alloys: Oxidation of Methanol and Ethanol. *Catal. Lett.* **2013**, (143), 636-641.
4. Yan, S. H.; Zhang, S. C.; Lin, Y.; Liu, G. R., Electrocatalytic Performance of Gold Nanoparticles Supported on Activated Carbon for Methanol Oxidation in Alkaline Solution. *J. Phys. Chem. C* **2011**, *115* (14), 6986-6993.
5. Boomi, P.; Prabu, H. G.; Mathiyarasu, J., Synthesis and characterization of polyaniline/Ag-Pt nanocomposite for improved antibacterial activity. *Colloid Surf. B-Biointerfaces* **2013**, *103*, 9-14.
6. Boomi, P.; Prabu, H. G.; Mathiyarasu, J., Synthesis, characterization and antibacterial activity of polyaniline/Pt-Pd nanocomposite. *Eur. J. Med. Chem.* **2014**, *72*, 18-25.
7. MacDiarmid, A. G.; Epstein, A. J., Polyanilines- A Novel Class of Conducting Polymers. *Faraday Discuss.* **1989**, *88*, 317-332.
8. Syed, A. A.; Dinesan, M. K., Review: Polyaniline-A Novel Polymeric Material *Talanta* **1991**, *38* (8), 815-837.
9. Sapurina, I. Y.; Shishov, M. A., Oxidative Polymerization of Aniline: Molecular Synthesis of Polyaniline and the Formation of Supramolecular Structures **2012**, 251-312.
10. Hatchett, D. W.; Josowicz, M.; Janata, J., Acid Doping of Polyaniline: Spectroscopic and Electrochemical Studies. *J. Phys. Chem* **1999**, *B* (103), 10992-10998.
11. Bhadra, S.; Khastgir, D.; Singha, N. K.; Lee, J. H., Progress in preparation, processing and applications of polyaniline. *Prog. Poly. Sci.* **2009**, *34*, 783-810.
12. Hatchett, D. W.; Josowicz, M.; Janata, J., Comparison of Chemically and Electrochemically Synthesized Polyaniline Films. *J. Electrochem. Soc.* **1999**, *146*, 4535-4538.
13. Polk, B. J.; Potje-Kamloth, K.; Josowicz, M.; Janata, J., Role of protonic and charge transfer doping in solid-state polyaniline. *J. Phys. Chem* **2002**, *106*, 11457-11462.
14. Mohilner, D. M.; Argersinger, W. J.; Adams, R. N., Investigation of Kinetics and Mechanism of Anodic Oxidation of Aniline in Aqueous Sulfuric Acid Solution at a Platinum Electrode. *J. Am. Chem. Soc.* **1962**, *84* (19), 3618-3622.
15. Agelopoulos, M.; Asturias, G. E.; Ermer, S. P.; Ray, A.; Scherr, E. M.; MacDiarmid, A. G.; Akhtar, M.; Kiss, Z.; Epstein, A. J., Polyaniline: Solutions, Films and Oxidation State. *J. Mol. Cryst. Liq. Cryst.* **1988**, *160*, 151-163.
16. Kinyanjui, J.; Wijeratne, N. R.; Hanks, J.; Hatchett, D. W., Chemical and electrochemical synthesis of polyaniline/platinum composites. *Electrochimica Acta* **2006**, *51*, 2825-2835.
17. Jozefowicz, M. E.; Epstein, A. J.; Tang, X., Protonic Acid Doping of 2 Classes of the Emeraldine Form of Polyaniline *Synth. Met.* **1992**, *46* (3), 337-340.
18. MacDiarmid, A. G.; Epstein, A. J., Secondary Doping in Polyaniline *Synth. Metals* **1995**, *69*, 85-92.

19. Hatchett, D. W.; Josowicz, M., Composites of Intrinsically Conducting Polymers as Sensing Nanomaterials. *Chem. Rev.* **2008**, *108*, 746-769.
20. Wang, J.; Neoh, K. G.; Kang, E. T., Preparation of Nanosized Metallic Particles in Polyaniline. *J. Colloid Interface Sci.* **2001**, *239* (1), 78-86.
21. Folarin, O. M.; Sadiku, E.; Maity, A., Polymer-noble metal nanocomposites: Review. *Int. J. Phys. Sci.* **2011**, *6* (21), 4869-4882.
22. Joo, J.; Oh, E. J.; Min, G.; MacDiarmid, A. G.; Epstein, A. J., Evolution of the conducting state of polyaniline from localized to mesoscopic metallic to intrinsic metallic regimes *Synth. Metals* **1995**, *69*, 251-254.
23. Stejskal, J.; Prokes, J.; Trchova, M., Reprotonation of polyaniline: A route to various conducting polymer materials. *React. Funct. Polym.* **2008**, *68*, 1355-1361.
24. Nagashree, K. L.; Ahmed, M. G., Electrocatalytic Oxidation of Methanol on Ni modified polyaniline electrode in alkaline medium. *Journal Solid State Electrochemistry* **2010**, *14*, 2307-2320.
25. Mao, H.; Wang, L.; Zhu, P.; Xu, Q.; Li, Q., Carbon-supported PdSnSnO<sub>2</sub> catalyst for ethanol electro-oxidation in alkaline media. *Inter. J. Hydrogen Energy* **2014**, *39*, 17583-17588.
26. Abdel Rahim, M. A.; Abdel Hameed, R. M.; Khalil, M. W., Nickel as a catalyst for the electro-oxidation of methanol in alkaline medium. *J. Power Sources* **2004**, *134*, 160-169.
27. Shafia Hoor, F.; Tharamani, C. N.; Ahmed, M. F.; Mayanna, S. M., Electrochemical synthesis of Fe–Mo and Fe–Mo–Pt alloys and their electrocatalytic activity for methanol oxidation. *J. Power Sources* **2007**, *167*, 18-24.
28. Shafei, A. A. E., Electrocatalytic oxidation of methanol at a nickel hydroxide/glassy carbon modified electrode in alkaline medium. *J. Electroanal. Chem.* **1999**, *471*, 89-95.
29. Huang, W.; Li, Z. L.; Peng, Y. D.; Chen, S.; Zheng, J. F.; Niu, Z. J., Oscillatory electrocatalytic oxidation of methanol on an Ni(OH)<sub>2</sub> film electrode. *J. Solid State Electrochem.* **2005**, *9* (5), 284-289.
30. Mostafaei, A.; Zolriasatein, A., Synthesis and characterization of conducting polyaniline nanocomposites containing ZnO nanorods. *Progress in Natural Science-Materials International* **2012**, *22* (4), 273-280.
31. Peng, H. L.; Liu, F. F.; Liu, X. J.; Liao, S. J.; You, C. H.; Tian, X. L.; Nan, H. X.; Luo, F.; Song, H. Y.; Fu, Z. Y.; Huang, P. Y., Effect of Transition Metals on the Structure and Performance of the Doped Carbon Catalysts Derived From Polyaniline and Melamine for ORR Application. *ACS Catal.* **2014**, *4* (10), 3797-3805.
32. Dimitriev, O. P., Doping of polyaniline by transition-metal salts. *Macromolecules* **2004**, *37* (9), 3388-3395.
33. Nagashree, K. L.; Ahmed, M. F., Electrocatalytic oxidation of methanol on Cu modified polyaniline electrode in alkaline medium. *J. Appl. Electrochem.* **2009**, *39*, 403-410.
34. Sharma, G.; Naushad, M.; Kumar, A.; Devi, S.; Khan, M. R., Lanthanum/Cadmium/Polyaniline bimetallic nanocomposite for the photodegradation of organic pollutant. *Iran. Polym. J.* **2015**, *24* (12), 1003-1013.
35. Ivanova, N. M.; Soboleva, E. A.; Visurkhanova, Y. A., Bimetallic Co-Cu polyaniline composites: Structure and electrocatalytic activity. *Russian Journal of Applied Chemistry* **2016**, *89* (7), 1072-1081.
36. Manzo-Robledo, A.; Costa, N. J. S.; Philippot, K.; Rossi, L. M.; Ramirez-Meneses, E.; Guerrero-Ortega, L. P. A.; Ezquerro-Quiroga, S., Electro-oxidation of methanol in

- alkaline conditions using Pd-Ni nanoparticles prepared from organometallic precursors and supported on carbon vulcan. *J. Nanopart. Res.* **2015**, *17* (12), 1-8.
37. Habibi, B.; Pournaghi-Azar, M. H.; Abdolmohammad-Zadeh, H.; Razmi, H., Electrocatalytic oxidation of methanol on mono and bimetallic composite films: Pt and Pt-M (M = Ru, Ir and Sn) nanoparticles in poly(o-aminophenol). *Int. J. Hydrog. Energy* **2009**, *34* (7), 2880-2892.
  38. Mahapatra, S.; Shekhar, S.; Thakur, B.; Priyadarshi, H., Synthesis and Characterization of Electrodeposited C-PANI-Pd-Ni Composite Electrocatalyst for Methanol Oxidation. *International Journal of Electrochemistry* **2014**, *2014*, 1-8.
  39. Yan, S. H.; Gao, L. Z.; Zhang, S. C.; Gao, L. L.; Zhang, W. K.; Li, Y. Z., Investigation of AuNi/C anode catalyst for direct methanol fuel cells. *Int. J. Hydrog. Energy* **2013**, *38* (29), 12838-12846.
  40. Rannabauer, S.; Schnick, W., Synthesis, Crstal Structure, and Spectroscopic Characterization of Bis(dimethylammonium) Hexachlorotitanate. *J. Natural Sci. B* **2003**, *58* (5), 410-410.
  41. Willard, H.; Merritt, L.; Dean, J.; Settle, F., *Instrumental Methods of Analysis*. 7th ed.; Wadsworth Inc.: Belmont, CA, 1988; p 182-183, 287-314.
  42. Skaarup, S.; Berg, R. W., Structural Properties and Vibrational Spectra of Ethylenediammonium Family of Perovskite Layer-type Crystals - NH<sub>3</sub>CH<sub>2</sub>CH<sub>2</sub>NH<sub>3</sub> MCl<sub>4</sub>, M=Ni, Pd, Cu, Cd, Mn. *J. Solid State Chem.* **1978**, *26* (1), 59-67.
  43. Tientong, J.; Garcia, S.; Thurber, C. R.; Golden, T. D., Synthesis of Nickel and Nickel Hydroxide Nanopowders by Simplified Chemical Reduction. *Journal of Nanotechnology* **2014**, *2014*, 1-7.
  44. Rifaya, N. M.; Theivasanthi, T.; Alagar, M., Chemical Capping Synthesis of Nickel Oxide Nanoparticles and their Characterization Studies *Journal of Nanoscience and Nanotechnology* **2012**, *2* (5), 1-11.
  45. Allerhand, A.; Schleyer, P. V., A Survey of C-H Groups as Proton Donors in Hydrogen Bonding *J. Am. Chem. Soc.* **1963**, *85* (12), 1715-1723.
  46. Harmon, K. M.; Gennick, I.; Madeira, S. L., Infrared Study of Cation C-H to Anion Hydrogen-Bonding and Crystal Habit in Tetramethylammonium Ion Salts *Abstr. Pap. Am. Chem. Soc.* **1974**, 31-31.
  47. Sutor, D. J., C-H ... O Hydrogen Bonds in Crystals. *Nature* **1962**, *195* (4836), 68-69.
  48. Nakanishi, K.; Goto, T.; Ohashi, M., Infrared Spectra of Organic Ammonium Compounds *Bull. Chem. Soc. Jpn.* **1957**, *30* (4), 403-408.
  49. Bottger, G. L.; Geddes, A. L., Infrared Spectra of Crystalline Tetramethylammonium Halides. *Spectrochimica Acta* **1965**, *21* (10), 1701-1708.
  50. Adams, D. M.; Gerratt, J.; Davidson, J. M.; Chatt, J., Far-Infrared Spectra (190-460 cm<sup>-1</sup>) of Tetraethylammonium Salts of Some Complex Chlorides and Bromides. *Journal of the Chemical Society* **1963**, (APR), 2189-2194.
  51. Goodgame, D. M.; Goodgame, M.; Weeks, M. J., Spectral and Magnetic Studies of Some Polymeric Complexes of Nickel Halides with Heterocyclic Ligands. *Journal of the Chemical Society* **1964**, (DEC), 5194-5199.
  52. Sabatini, A.; Sacconi, L., Far-Infrared Spectra of Some Tetrahalo Metal Complexes *J. Am. Chem. Soc.* **1964**, *86* (1), 17-20.



53. Omura, Y.; Shimanouchi, T., Infrared-Spectra and Rotational-Isomerism of Ethylenediammonium Ion in Aqueous-Solution. *Journal of Molecular Spectroscopy* **1973**, *45* (2), 208-220.
54. Omura, Y.; Shimanouchi, T., Raman-Spectra and Rotational-Isomerism of Ethylenediammonium and Monoethanolammnoium Ions in Aqueous-Solution. *Journal of Molecular Spectroscopy* **1975**, *55* (1-3), 430-434.
55. Griffiths, T. R.; Scarrow, R. K., Effects of Cations upon Absorption Spectra. Parts 2-3. *Trans. Faraday Soc.* **1969**, *65* (559P), 1727-1734.
56. Gill, N. S.; Nyholm, R. S., Complex Halides of the Transition Metals.1. Tetrahedral Nickel Complexes *Journal of the Chemical Society* **1959**, (DEC), 3997-4007.
57. Bartosik, J.; Mudring, A. V., [Ni(tmen)(acac)][B(Ph)<sub>4</sub>] a Probe for the Anion Basicity of Ionic Liquids. *Physical Chemistry Chemical Physics* **2010**, *12*, 4005-4011.
58. Angell, C. A.; Gruen, D. M., Octahedral-Tetrahedral Coordination Equilibria of Nickel(II) and Copper(II) in Concentrated Aqueous Electrolyte Solutions. *Journal of American Chemical Society* **1966**, *88* (22), 5192-5198.
59. Cotton, F. A.; Faut, O. D.; Goodgame, D. M. L., Preparation, Spectra and Electronic Structures of Tetrahedral Nickel(II) Complexes Containing Triphenylphosphine and Halide Ions as Ligands. *Journal of American Chemical Society* **1961**, *83* (2), 344-351.
60. Gruen, D. M.; McBeth, R. L., Tetrahedral NiCl<sub>4</sub><sup>-</sup> Ion in Crystals and in Fused Salts. Spectrophotometric Study of Chloro Complexes of Ni(II) in Fused Salts. *Journal of Physical Chemistry* **1959**, *63* (3), 393-398.
61. Liu, W. H.; Migdisov, A.; Williams-Jones, A., The stability of aqueous nickel(II) chloride complexes in hydrothermal solutions: Results of UV-Visible spectroscopic experiments. *Geochim. Cosmochim. Acta* **2012**, *94*, 276-290.
62. Wu, M. Q.; Gao, J. H.; Zhang, S. R.; Chen, A., Comparative studies of nickel oxide films on different substrates for electrochemical supercapacitors. *Journal of Power Sources* **2006**, *159* (1), 365-369.
63. Ciszewski, A.; Sron, K.; Stepniak, I.; Milczarek, G., Nickel (II) lignosulfonate as precursor for the deposition of nickel hydroxide nanoparticles on a glassy carbon electrode for oxidative electrocatalysis. *Electrochimica Acta* **2014**, *134*, 355-362.
64. Teo, W. Z.; Pumera, M., Simultaneous Direct Voltammetric Determination of Metal-Oxide Nanoparticles from Their Mixture (CuO/NiO). *ChemElectroChem* **2014**, *1* (1), 249-253.
65. Fleischmann, M.; Korinek, K.; Pletcher, D., The Oxidation of Organic Compounds at a Nickel Anode in Alkaline Solution. *J. Electroanal. Chem.* **1971**, *31*, 39-49.
66. Giovanni, M.; Ambrosi, A.; Pumera, M., The Inherent Electrochemistry of Nickel/Nickel-Oxide Nanoparticles. *Chem.-Asian J.* **2012**, *7* (4), 702-706.
67. Visscher, W.; Barendrecht, E., THE ANODIC-OXIDATION OF NICKEL IN ALKALINE-SOLUTION. *Electrochimica Acta* **1980**, *25* (5), 651-655.
68. Menezes, P. W.; Indra, A.; Levy, O.; Kailasam, K.; Gutkin, V.; Pfromm, J.; Driess, M., Using nickel manganese oxide catalysts for efficient water oxidation. *Chem. Commun.* **2015**, *51*, 5005-5008.
69. Fominykh, K.; Feckl, J. M.; Sicklinger, J.; Doblinger, M.; Boecklein, S.; Ziegler, J.; Peter, L.; Rathousky, J.; Scheidt, E.-W.; Bein, T.; Fattakhova-Rohlfing, D., Ultrasmall Dispersible Crystalline Nickel Oxide Nanoparticles as High-Performance Catalysts for Electrochemical Water Splitting. *Adv. Funct. Mater.* **2014**, *24*, 3123-3129.

70. Gao, M.; Sheng, W.; Zhuang, Z.; Fang, Q.; Gu, S.; Jiang, J.; Yan, Y., Efficient Water Oxidation Using Nanostructured  $\alpha$ -Nickel-Hydroxide as an Electrocatalyst. *J. Amer. Chem. Soc.* **2014**, *136*, 7077–7084.
71. Trotochaud, L.; Ranney, J. K.; Williams, K. N.; Boettcher, S. W., Solution-Cast Metal Oxide Thin Film Electrocatalysts for Oxygen Evolution. *J. Am. Chem. Soc.* **2012**, *134*, 17253–17261.
72. Nikiforova, T. G.; Stepanova, A. A.; Datskevich, O. A., Porous Nickel Deposits Formed in the Oxidation of Alcohols in an Alkaline Medium. *Russ. J. Appl. Chem.* **2013**, *86*, 1713-1715.
73. Tong, X. L.; Qin, Y.; Guo, X. Y.; Moutanabbir, O.; Ao, X. Y.; Pippel, E.; Zhang, L. B.; Knez, M., Enhanced Catalytic Activity for Methanol Electro-oxidation of Uniformly Dispersed Nickel Oxide Nanoparticles-Carbon Nanotube Hybrid Materials. *Small* **2012**, *8* (22), 3390-3395.
74. Shamsipur, M.; Najafi, M.; Hosseini, M. R. M., Electrooxidation of alcohols at a nickel oxide/multi-walled carbon nanotube-modified glassy carbon electrode. *Journal of Applied Electrochemistry* **2013**, *43* (10), 1027-1033.
75. Elzatahry, A., Polyacrylonitril Electrospun Nanofiber As a Template to Prepare NiO Nanostructure Electrocatalyst. *Int. J. Electrochem. Sci.* **2014**, *9* (1), 22-31.
76. El-Shafei, A. A., Electrocatalytic oxidation of methanol at a nickel hydroxide/glassy carbon modified electrode in alkaline medium. *Journal of Electroanalytical Chemistry* **1999**, *471* (2), 89-95.
77. Chen, A. C.; Lipkowski, J., Electrochemical and spectroscopic studies of hydroxide adsorption at the Au(111) electrode. *J. Phys. Chem. B* **1999**, *103* (4), 682-691.
78. Mierczynski, P.; Vasilev, K.; Mierczynska, A.; Maniukiewicz, W.; Szykowska, M. I.; Maniecki, T. P., Bimetallic Au-Cu, Au-Ni catalysts supported on MWCNTs for oxy-steam reforming of methanol. *Appl. Catal. B-Environ.* **2016**, *185*, 281-294.
79. Yang, F.; Yao, Y. X.; Yan, Z.; Min, H.; Goodman, D. W., Preparation and characterization of planar Ni-Au bimetallic model catalysts. *Appl. Surf. Sci.* **2013**, *283*, 263-268.
80. Kirk, D. W.; Foulkes, F. R.; Graydon, W. F., The Electrochemical Formation of Au(I) Hydroxide on Gold in Aqueous Potassium Hydroxide *Journal of the Electrochemical Society* **1980**, *127* (5), 1069-1076.

## Curriculum Vitae

Graduate College  
University of Nevada, Las Vegas

Morgan Emily Pacini

E-mail address: Mejarvis4@gmail.com

### Degrees:

Bachelor of Science – Biochemistry, 2013  
University of Nevada, Las Vegas

### Thesis Title:

Synthesis and Electrochemical Characterization of PANI/Ni and PANI/Au/Ni  
Composites

### Thesis Examination Committee:

Chairperson, Dr. David W. Hatchett, Ph.D.  
Committee Member, Dr. Spencer Steinberg, Ph.D.  
Committee Member, Dr. Bryan Spangelo, Ph.D.  
Graduate Faculty Representative, Dr. Terry Spell, Ph.D.